Ecological Indicators 175 (2025) 113509

Contents lists available at ScienceDirect

Ecological Indicators

journal homepage: www.elsevier.com/locate/ecolind

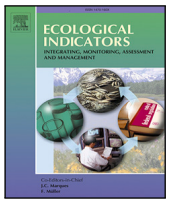

# Simulated fire observables as indicators for optimizing wireless sensor networks in wildfire risk monitoring

Juan Luis Gómez-González [a,b,*], Effie Marcoulaki [b], Alexis Cantizano [a], Myrto Konstantinidou [b], Raquel Caro [c], Mario Castro [a,d]

[a] Institute for Research in Technology (IIT), ICAI School of Engineering, Comillas Pontifical University, c/ Rey Francisco, 4, 28008, Madrid, Spain
[b] System Reliability and Industrial Safety Laboratory, Institute of Nuclear & Radiological Sciences & Technology, Energy & Safety, National Centre for Scientific Research "Demokritos", 15310 Ag. Paraskevi, Attiki, Athens, 60037, Greece
[c] University Institute of Studies on Migration (IUEM), Chair in Disasters Fundación AON, España, c/ Rey Francisco, 4, 28008, Madrid, Spain
[d] Grupo Interdisciplinar de Sistemas Complejos (GISC), Comillas Pontifical University, c/ Alberto Aguilera, 25, 28008, Madrid, Spain

ARTICLE INFO

*Keywords:*
Wildfire simulation
Optimization
Early wildfire detection system
Wireless sensor network
NSGA-II

ABSTRACT

Uncontrolled wildfires cause significant damage and economic costs. Wireless Sensor Networks (WSNs) can mitigate these impacts by detecting fires early across extensive wildland areas. This work presents a simulation-driven optimization framework for localizing WSNs to enhance early wildfire detection and minimize potential damage. Formulated as a Multi-Objective Optimization Problem (MOOP) and solved using the Non-dominated Sorting Genetic Algorithm II (NSGA-II), the method utilizes dynamic wildfire simulations and considers stochastic variables such as ignition likelihood and weather conditions. The methodology is general and independent of the simulation model or the studied region. The framework supports decision-making under uncertainty, ensuring the designed networks remain effective across varying conditions. A practical case study with validated fire behaviour demonstrates the robustness of the approach to identify the most efficient and cost-effective sensor locations. Results show significantly better performance compared to uniform sensor grids and WSNs designed for fixed-weather scenarios, highlighting the benefits of this approach for wildfire management.

## 1. Introduction

Uncontrolled wildfires represent one of the most pernicious natural disasters as they bring significant ecological (De Oliveira et al., 2023; Dupuy et al., 2020; Hoffman et al., 2021; Mack et al., 2021; Van Der Werf et al., 2017), economic (Bayham et al., 2022; Marshall et al., 2023; Meier et al., 2023), and social (Machado-Silva et al., 2020; Molina-Terrén et al., 2019; Pan et al., 2023; De Diego et al., 2023) costs. Active suppression—encompassing detection, response, containment, and control—is mandatory to tackle the spread of undesired fire events and mitigate their adverse impacts (Plucinski, 2019). The dimension and shape of a wildfire (e.g., burnt area and perimeter-to-area ratio) are highly related to the wildland fire suppression expenditures (Calkin et al., 2005; Gebert et al., 2007; Liang et al., 2008). Therefore, given the exponential growth of fast fires, fast response times are necessary to mitigate costs and damage (Rodrigues et al., 2019). Adopting Early Wildfire Detection Systems (EWDS) is a promising solution to shorten the response phase.

Their use (Mohapatra and Trinh, 2022) integrates a network of elements that collectively monitor large areas with minimum human intervention (Carta et al., 2023). These interconnected elements include sensor nodes, unmanned aerial vehicles (UAVs), optical cameras, and satellite surveillance. The low costs of the Internet of Things (IoT) devices and the consolidation of communication improvements such

*Abbreviations:* AT, Arrival Time; BA, Burnt Area; CA, Cellular Automata; DBA, Detected Burnt Area; ECMWF, European Centre for Medium-Range Weather Forecasts; EFFIS, European Forest Fire Information System; ETRS89, European Terrestrial Reference System 1989; ERA5, Fifth Generation ECMWF Reanalysis for the Global Climate and Weather; EWDS, Early Wildfire Detection System; FSF, Free-Spreading Fire; FWI, Fire Weather Index; GA, Genetic Algorithms; IoT, Internet of Things; LBPM, Landscape Burnt Probability Map; MOOP, Multi-Objective Optimization Problem; NSGA-II, Non-Dominated Sorting Genetic Algorithm II; SIGIF, Integrated Forest Fire Management System of Generalitat Valenciana; WII, Wildland Industrial Interface; WSN, Wireless Sensor Network; WUI, Wildland Urban Interface.

* Corresponding author at: Institute for Research in Technology (IIT), ICAI School of Engineering, Comillas Pontifical University, c/ Rey Francisco, 4, 28008, Madrid, Spain.
*E-mail address:* jgomezg@comillas.edu (J.L. Gómez-González).
*URL:* https://www.iit.comillas.edu/personas/jgomezg (J.L. Gómez-González).

https://doi.org/10.1016/j.ecolind.2025.113509
Received 9 December 2024; Received in revised form 2 April 2025; Accepted 17 April 2025
Available online 17 May 2025

as 5G have catalyzed the implementation of these systems in recent years. The integration of physical signal recording and edge computing enables processing a wide array of wildfire influencing factors, including temperature, humidity, precipitation, wind speed, air pressure, light intensity, and concentration of smoke particles and combustion gases (e.g., $CO_2$, CO) (Sairi et al., 2023).

Static Wireless Sensor Networks (WSNs) are energy-efficient, cost-effective, readily scalable, adaptable to heterogeneous environments, and reliable for real-time monitoring (Yick et al., 2008). Their application for the wildland-forest environment involves specifying various aspects of sensor devices, communication frameworks, and system design to address energy consumption efficiency (Kaur et al., 2023), the appropriate IoT communications protocols (Chan et al., 2023), edge computing for processing the environmental data (Kizilkaya et al., 2022), and sensor calibration methodologies for accurate fire detection (Dampage et al., 2022). Commercial implementations underscore the importance of environmentally conscious solutions (Dryad Networks, 2025; Pyri, 2025).

The standard deployment strategy typically follows a uniform pattern, either through random placement—adjusting sensor density based on fuel distribution and topography to maintain effective communication (Lloret et al., 2009; Verma et al., 2021)—or through deterministic coverage of the entire area (Aslan et al., 2012). A mathematical optimization approach could minimize installation and operational costs without compromising early detection performance.

Optimization requires large volumes of high-quality fire behaviour data to produce accurate and realistic recommendations. However, data from past or experimental fires are unsuitable, as changes in the landscape alter subsequent fire behaviour (Hantson et al., 2022). Instead, when properly parameterized with detailed geospatial information, operational wildfire models offer fast and reliable predictions across a broad range of scenarios (Sullivan, 2009), supplying the necessary input to optimize the sensor locations.

Environmental modelling and geospatial data have been used in different optimization applications including the routing of pipelines (Skretas et al., 2022), the placement of watchtowers for early wildfire detection (Heyns et al., 2019), and the design of ecological corridors (Dang et al., 2024). In fire management, wildfire simulations support the optimal planning of firebreaks (Carrasco et al., 2023), fuel treatment strategies (Arca et al., 2015; Karimi et al., 2024), and fire suppression operations (Granda and Vitoriano, 2024).

This work integrates dynamic wildfire simulations into optimizing WSN localization for early wildfire detection. An extensive literature survey revealed only one study specifically addressing sensor placement for optimal wildfire detection (Azevedo et al., 2021) focused on sensor coverage based on distance and local forest density without considering wildfire dynamics. The use of simulations to optimize the placement of sensors has been applied in groundwater pollution monitoring (Bode et al., 2019) where a similar approach was proposed. Our contribution also incorporates probabilistic information on wildfire scenarios and supports a variety of criteria for the cost and the operational performance of the WSN.

The paper's outline is as follows: Section 2 summarizes the methodology and describes the optimization approach. Section 3 illustrates the case study, introduces simulation data, discusses the problem discretization, and defines the set of meteorological scenarios. Section 4 presents the results of our proof-of-concept, and Section 5 details the implications of the findings. Finally, Section 6 concludes this work.

## 2. WSN optimization methodology

Our methodology aims to determine the optimal placement of static sensors for early detection of wildfires. According to Fig. 1, the optimization problem is formulated as follows:

Given:

- Spatio-temporal simulations for potential wildfire scenarios,
- Probabilities for each wildfire scenario to materialize,
- A grid of predefined candidate sensor locations, and
- Objectives and constraints on the wildfire attributes upon detection;

Determine which are the optimal sensor locations in the grid.

In the following subsections, we describe the optimization framework for the sensor location problem and its implementation. Also, we describe how we set up and simulate the wildfire scenarios to evaluate the WSN performance using alternative formulations of objectives and constraints.

### 2.1. Optimization background

In this work, determining the optimal sensor locations constitutes a Multi-Objective Optimization Problem (MOOP), generally formulated as follows:

$$\text{minimize} \quad \vec{F}(s) = \left(f_1(s), f_2(s), \dots, f_N(s)\right) \quad \text{with} \quad s \in \Omega, \tag{1}$$

$$\text{s.t.} \quad \vec{G}(s) = \left(g_1(s), g_2(s), \dots, g_M(s)\right) \leq 0 \tag{2}$$

where $s$ denotes a particular solution (in our case, which locations on the grid should contain a sensor) and $\Omega$ is the domain of feasible solutions. The overall performance of $s$, $\vec{F}(s)$, is a vector containing $N$ criteria, $f_n(s), n = 1, 2, \dots, N$. The objective here is to find solutions that minimize simultaneously all the $N$ criteria while satisfying the $M$ constraints $g_m(s), m = 1, 2, \dots, M$ in $\vec{G}(s)$.

When we have conflicting criteria, we cannot find a single optimal solution that minimizes all of them. In this case, the optimum is the set of all feasible solutions that meet the Pareto-optimality principle: it is impossible to improve any solution in the Pareto set in terms of one criterion without worsening one or more of the other criteria. In the case of bi-objective problems, the Pareto set can be plotted on the $(f_1(s), f_2(s))$ plane to indicate the ultimate boundary curve, called the Pareto front.

### 2.2. WSN performance evaluation

Fig. 2 shows the progress of four fires starting from two ignition locations (top-left for a and c, and bottom-central for b and d) under two wind fields (North-West winds in a and b, and East winds in c and d). We also consider that we have deployed a WSN in this area. As expected, the WSN performs differently in each fire, in terms of the fire detection time, the burnt area or the fire front at the time of detection. In scenario a, a sensor is located in the direction of fire spread, enabling detection in 2.5 h. In scenario c, the fire pattern changes due to winds blowing towards the West direction and a different sensor is triggered, delaying the detection time to 4 h. Fires b and d are detected again within 2,5 h and 4 h hours, but by different sensors, although they started from the same locations as a and b, respectively. This section discusses how we can evaluate the performance of any given WSN, like the ones in Fig. 2 using data from wildfire simulations.

Using a realistic fire spread model, it is possible to predict wildfire attributes detectable by a WSN, and optimize its design using an ensemble of (known) ignition points. Examples of such attributes are the propagation of the fire perimeter, the dispersion of combustion gases, the atmospheric transport smoke particles and embers, heat release, the sound made by the burning process, among others (Prieto Herráez et al., 2017; Coen et al., 2013; Finney, 1998; Linn et al., 2002; Prichard et al., 2014; Ottmar, 2014; Tymstra et al., 2010). In a real case scenario, the optimal sensor localization should consistently perform well regardless of the ignition location and the weather conditions during a wildfire and inform the authorities about the existence of an unexpected fire.

In summary, we characterize our fire simulations dataset according to:

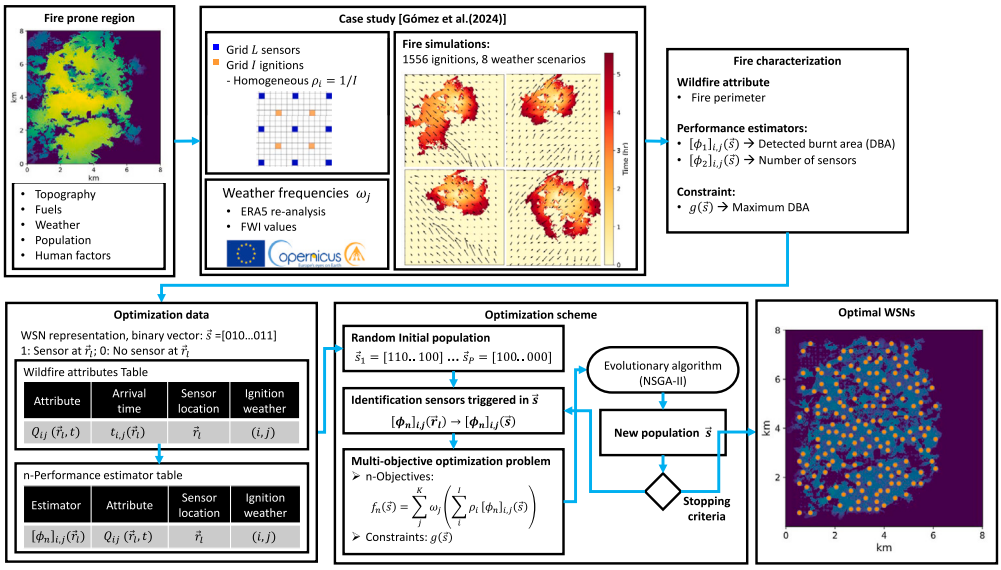


**Fig. 1.** The panel illustrates the optimization process, starting with the generation of fire simulation data, the design of the grid for candidate sensor locations, and the problem formulation discussed later.

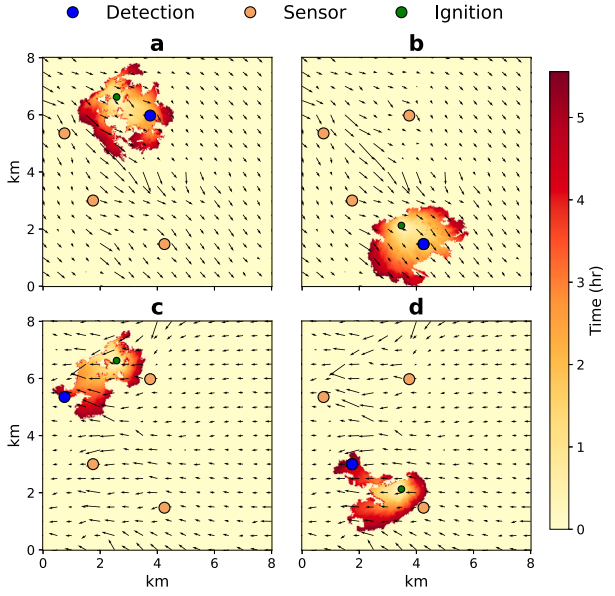


**Fig. 2.** Fire simulations corresponding to two sets of ignition points (identical for a, c, and correspondingly b, d) and wind distributions (a,b North-West winds, c,d East winds). Wind fields were produced with WindNinja (Wagenbrenner et al., 2016). Note how different initial and weather conditions change the early detection capability of the WSN.

- A given set of $I$ ignition points, and their occurrence probabilities $\rho_i$, $i \in [1, I]$, s.t. $\sum_i \rho_i = 1$.
- A given set of $K$ weather conditions, and their frequencies $\omega_j$, $j \in [1, K]$, s.t. $\sum_j \omega_j = 1$.

We simulate for each ignition location $i$ and weather scenario $j$ the wildfire observable threshold that triggers a sensor placed at a position $\vec{r}$ at time t, which we note $Q_{i,j}(\vec{r}, t)$. Using the simulation datasets, we can compute the optimization criteria and constraints (see Eqs. (1)–(2)). In particular, given a WSN arrangement $s$, we apply a set of user defined functions $h_n$, to evaluate its performance $[\phi_n]_{i,j}$ based on the fire simulation data:

$$[\phi_n]_{i,j}(s) = h_n\left(Q_{i,j}(\vec{r}, t), s\right) \tag{3}$$

Each criterion $f_n(s)$ considers the overall performance of design $s$ with respect to each function $[\phi_n]_{i,j}$. The performance of each scenario $(i, j)$ contributes to $f_n(s)$ according to the following correlation, factoring in the frequency of weather conditions and the probability of each ignition point in the studied area:

$$f_n(s) = \sum_j^K \omega_j \left( \sum_i^I \rho_i \left[\phi_n\right]_{i,j}(s) \right) \tag{4}$$

The performance functions, $h_n$, can be defined according to the specific prevention goals of each case study.

- Informing of an uncontrolled fire as soon as possible, then $h_n$ corresponds to the detection times following the signal triggering the sensors.
- Reducing the damage caused by the fire, for which adequate candidates for $h_n$ are burnt area or fire perimeter after detection, regardless of the time fire spreads.
- Minimizing specific losses at detection (e.g. biodiversity, economical, carbon emissions) for which $h_n$ should include additional information about the burnt elements (e.g. Wildland-Urban/Industrial interfaces mappings (WUI/WII), or tabulated emissions release by combusted fuel type).

Additional criteria intrinsic to the sensor technology, like the WSN installation and maintenance costs, can be considered.

We may also impose constraints on the fire attributes or the network characteristics according to Eq. (2), such as thresholds on the number of sensors, the maximum undetected damage, or levels of risk avoidance in strategic/valuable areas.

### 2.3. Numerical implementation

The optimization approach utilizes a large amount of simulation data, requiring careful mathematical encoding to reduce the computational load. During evaluation over $I$ and $K$ sets, sensors are static, thus the solutions $s$ encode the location of sensors in the network. To simplify the combinatorial explosion, candidate sensor locations are restricted to a set $\vec{r}_l$, $l \in [1, L]$. Therefore, the optimization variables constitute a binary vector, $\vec{s} = \{s_l\}$, denoting the presence ($s_l = 1$) or not ($s_l = 0$) of a sensor at candidate location $\vec{r}_l$.

The *arrival times* (AT), $t_{i,j}(\vec{r})$, define the time intervals relative to the ignition instant required to trigger a sensor placed at the candidate

location $\vec{r}$. These values are static regardless of the dissipation of the wildfire attributes $Q_{i,j}(\vec{r},t)$ triggering the sensors (e.g. smoke concentration build-up necessary to trigger a sensor and subsequent dissipation). From the detection point of view, the most critical variable is the time when the first sensor is triggered, denoted here as $t_{i,j}^{\text{detection}}(\vec{s})$. For a candidate $\vec{s}$ and given simulation conditions (weather, ignition location), this time is the minimum of ATs to any sensor in the network:

$$t_{i,j}^{\text{detection}}(\vec{s}) = \min_{l}\{t_{i,j}(\vec{r}_l) \mid s_l = 1\} \tag{5}$$

The computational efficiency of the optimization process improves providing the sensor candidate locations sorted by increasing ATs for each wildfire simulation. Then, the sensor that detects a wildfire is the first element of the sorted list such that $s_l = 1$. Once the detection is identified by a particular sensor, it is necessary to derive the performance functions $h_n$. For simplification, we introduce the notation of $\vec{s}_l$ as the configuration with a single sensor (i.e. size one) located at the candidate position $\vec{r}_l$. Thus, the total necessary fire data consists of two tables, one listing the sorted candidate sensor locations and another corresponding to the $[\phi_n]_{i,j}(\vec{s}_l)$ values. The sorted candidate sensor locations enable the use of post-detection applications with low computational costs, as the sequence of sensors triggering the fire detection is readily accessible.

We assume that the WSN fails to detect the fire if the simulation time exceeds a given threshold. In reality, such fires would probably be detected by human observation or other detection systems, but much later. In those cases, we consider that a non-detected fire has to be penalized due to that failure to trigger an alert on time. The penalization assigns the final simulated time and maximum performance criteria $h_n$ (e.g., total burnt area, final fire perimeter, the highest concentration of combustion gases, etc.) to those candidate sensor locations not experiencing the arrival of $Q_{i,j}(\vec{r},t)$. This penalty scales with the severity of the wildfire, which effectively diminishes the weight of non-dangerous fires in the optimization process, ensuring the system prioritizes the detection of potentially destructive fires.

Constraints presented in Eq. (2) are problem-dependent. When these impose upper limits on $h_n$ performance criteria values, they can be computed in parallel to the performance objectives $f_n$ by subtracting the difference between $[\phi_n]_{i,j}$ and the thresholds provided. These differences accumulate when a constraint is unmet, representing the restriction's deviation. The optimizer then uses this information to improve the search for solutions that fulfil the constraint.

### 2.4. Non-dominated sorting genetic algorithm II and Pymoo

The problem formulation considered here has only binary variables and the objective functions/constraints are discontinuous and nonlinear. For these types of problems, Genetic Algorithms (GA) appear as an excellent choice and have been used in similar applications in wildfire management and sensor optimization (Chen et al., 2022; Arca et al., 2015; Castro et al., 2024; Azevedo et al., 2021). GA consider a population of solutions that are modified using operations like crossover and mutation from one iteration of the algorithm (i.e. generation) to the next one. We use here the Non-dominated Sorting Genetic Algorithm II (NSGA-II) (Deb et al., 2002) implemented in Pymoo (Blank and Deb, 2020). Pymoo is a Python-based optimization framework that provides advanced single- and multi-objective optimization algorithms, as well as visualization and decision-making support. In NSGA-II, only a fraction of the population is actually modified (i.e., offspring population) to ensure that we reach a set of non-dominated solutions. NSGA-II employs a fast sorting approach to classify the solution populations into different levels of Pareto fronts. NSGA-II also incorporates a crowding distance mechanism to preserve solution diversity within the same front, ensuring a well-distributed Pareto-optimal front. NSGA-II is suitable for bi-objective problems, and additional criteria can be introduced as constraints (Skretas et al., 2022). Deb et al. (2002) provided detailed information on how NSGA-II generates a good approximation of the Pareto front. Algorithm 1 outlines the optimization pipeline proposed in this work and where we need to call the NSGA-II routine.

**Algorithm 1** Numerical implementation of the optimization framework.

**Input:** $Q_{i,j}(\vec{r},t)$, $\rho_i$, $\omega_j$, candidate sensor locations $\vec{r}_l$
**Output:** Pareto-optimal front WSNs, $\vec{s}$
Define objectives $f_n(\vec{s})$
Define constraints $g_m(\vec{s})$
**Initialize arrival time (AT) and performance functions for all candidate sensor locations**
**for** each ignition $i \in I$ **do**
  **for** each weather $j \in K$ **do**
    **for** each $\vec{r}_l$, $l \in L$ **do**
      **if** $Q_{i,j}(\vec{r}_l,t)$ arrives **then**
        Compute $t_{i,j}(\vec{r}_l)$
        Compute $[\phi_n]_{i,j}(\vec{s}_l)$
      **else** $Q_{i,j}(\vec{r}_l,t)$ does not arrive
        Penalize $\vec{r}_l$ with $\max\{t_{i,j}(\vec{r}_l)\}$
        Penalize $\vec{r}_l$ with $\max\{[\phi_n]_{i,j}(\vec{s}_l)\}$
      **end if**
    **end for**
    Sort $\vec{r}_l$ by increasing $t_{i,j}(\vec{r}_l)$
    Store sorted candidate sensor locations and $[\phi_n]_{i,j}(\vec{s}_l)$
  **end for**
**end for**
**Call the optimizer (see Section 2.4)**
  Default optimizer initialization (Blank and Deb, 2020)
  **for** each generation **do**
    **for** each WSN configuration $\vec{s}$ in population **do**
      Evaluate criteria and constraints (Eqs. (7), (8), (9))
    **end for**
    Generate the next population of solutions
  **end for**
**Return** Pareto front optimal WSN

### 2.5. Example of objectives and constraints formulation

Our criteria to find the best WSN are based on evaluating the performance of solutions $\vec{s}$, comprising a static layout of sensors, denoted as $t_{i,j}^{detection}(\vec{s})$. Geographical information systems provide spatial characterization of wildland domains as rasters. To illustrate our methodology, we assume that due to the limited spatial resolution provided by the raster format, the sensors detect the fire (and trigger the corresponding signal) deterministically whenever the wildfire perimeter reaches the pixel where these are located. More information about the fire simulator used to reproduce these dynamics is explained in Section 3.2.

In this section we present a practical example where the WSN optimization is formulated as a bi-objective problem. The example considers a performance-related objective function and a cost-related objective function. Further requirements are included as operational constraints, as explained below. The results of Section 4 are obtained using this example formulation.

#### 2.5.1. Performance-related objective function

Fire size and shape are the main indicators of negative impacts and economic costs (Calkin et al., 2005; Gebert et al., 2007; Liang et al., 2008). Therefore, in the current implementation, we propose to overlook the detection time and minimize Burnt Areas (BA) at detection. Prioritizing the BA intrinsically reduces the importance of non-dangerous fires in the optimization process and ensures that the network effectively targets potentially destructive fires. Therefore, to build a first objective, we propose to target BA for each specific ignition and meteorological scenario at detection time as the performance function $h_1$, which depends on $\vec{s}$

$$BA_{i,j}\left(t_{i,j}^{\text{detection}}(\vec{s})\right) = [\phi_1]_{i,j}(\vec{s}) = h_1\left(Q_{i,j}(\vec{r}, t_{i,j}^{\text{detection}}), \vec{s}\right) \tag{6}$$

The global performance objective, $f_1(s)$ aggregates individual fire detection assessments by the solution $\vec{s}$ as presented in Eq. (4)

$$f_1(s) = \sum_j^W \omega_j \left( \sum_i^I \rho_i BA_{i,j} \left( t_{i,j}^{\text{detection}}(\vec{s}) \right) \right) \tag{7}$$

The performance objective Eq. (7) has the clear physical meaning of minimizing the average Detected Burnt Area (DBA) across all weather scenarios and ignitions. The algorithm showing the computation of $f_1$ according to the numerical implementation is part of the supplementary material.

#### 2.5.2. Cost-related objective function

We also aim to minimize the size of the network and reduce the costs (and difficulties) inherent to the deployment, maintenance, and purchasing of the sensors. In the absence of detailed data, these costs could be assumed to be proportional to the size of the grid of candidate sensor locations, so

$$f_2(\vec{s}) = \sum_l^L s_l \tag{8}$$

The algorithm showing the computation of $f_2$ is part of the supplementary material.

#### 2.5.3. Operational constraints

A final element of the optimization is the set of constraints $\vec{G}(\vec{s})$. In Spain, the potential severity index of a forest fire (ranging from 0 to 3 in increasing severity) is an essential metric for managing the resources and means mobilized during an emergency (Ministerio del Interior, Secretaría General Técnica, Dirección General de Protección Civil y Emergencias, 2014). In particular, level 0 implies that the wildfire is suppressed with local capacity, and levels 1 to 3 set increasing fire risk scenarios demanding the dispatch of extraordinary resources. The conditions leading to different potential severity index classes are defined at the Spanish regional administration level. In particular, the Civil Protection plans of the region "Castilla *y* León" state that fires burning more than 30 ha fit the potential severity index level 1 and higher (Gobierno de Castilla y León, 1999). The specification of potential severity indexes based on wildfire attributes poses an opportunity to define constraints able to provide confidence that optimal WSNs operate under operational demands. In our study, the optimization considers various DBA constraints (Eq. (9)), including the cited 30 ha, which is the upper limit for an undetected fire.

$$g_1\left(\vec{s}\right) \equiv BA_{i,j}\left(t_{i,j}^{\text{detection}}(\vec{s})\right) - BA_g \leq 0 \quad \forall i \in I, \forall j \in K \tag{9}$$

For details on the code and access to the simulated data tables necessary to run the case study of this work, we refer to Section "Software and data availability".

## 3. Simulation data

This study focuses on a case study located in Spain that experienced a severe wildfire incident in 2012. We use a propagation model previously validated in this specific scenario to conduct our wildfire simulations (Gómez-González et al., 2024). Meteorological data for the simulations are sourced from the COPERNICUS ERA5 dataset (Copernicus Climate Change Service (C3S), 2018), along with the procedure to identify the different high-danger fire-weather conditions and their frequencies to run the simulations. Wind fields were produced with WindNinja (Wagenbrenner et al., 2016).

### 3.1. Case study data

The area of study refers to a region in the outskirts of Cocentaina, a small town in the province of Alicante, South-East Spain. The forested area corresponds to the "Protected Natural Area of Mariola Mountain Range". The landscape model reproduces conditions before a severe wildfire incident that happened in 2012. Fire behaviour variables were computed in a previous work (Gómez-González et al., 2024), with a representation of the elevations map and surface fuel distribution shown in Fig. 3-left, 3-right respectively.

The wildfire's evolution, weather conditions, and final burnt area were documented by the "Integrated Wildland Fire Management System" (SIGIF) from the Spanish Autonomous Region of Valencia (Generalitat Conselleria de Medio Ambiente, Infraestructuras y Territorio, 2015). The conditions leading to the Cocentaina 2012 wildfire incident are representative of the high fire susceptibility characterizing this mediterranean landscape. During the period from 1995 to 2019, the region experienced 88 fire outbreaks, out of which 18 escaped initial suppression (Ministerio para la Transición Ecológica y el Reto Demográfico (MITECO), 2019), supporting the future adoption of EWDS. Because of the proximity of the municipality of Cocentaina to the fire ignition, the municipal boundary is integrated into the fire domain used in this work. Thus, the fire landscape constitutes an example of a WUI scenario.

### 3.2. Fire simulations

The fire simulator used to produce fire dynamics data required for optimizing WSN configurations is taken from Gómez-González et al. (2024). This model was validated on the fire domain described in the case study. Fire growth is prescribed considering Cellular Automata (CA) modelling based on the cells comprising a raster representation of the fire domain. The CA models the combustion state of fuel elements with a single possible transition from unburnt to burning states, predicting burnt area growth over time.

Here, we consider only fires initiated from single ignition sources. We also assume the meteorological and environmental conditions remain constant between the fire ignition and the fire detection. To provide enough fire propagation data, our simulation experiments run 5 real-time hours.

### 3.3. Domain discretization: distribution of ignition and sensor points

The fire scenario comprises an area of 6441 ha, with an intricate distribution of fuel type, canopy structure, moisture, wind, etc, including the WUI with the municipality of Cocentaina. To accommodate the environment variability, the domain is segmented on a squared lattice of cells of size $25 \times 25\,\text{m}^2$, including $321 \times 321$ cells in total. The methodology is tested only on the portion of the fire domain located west of the town, covering 4110 ha.

This study assumes the probability of an uncontrolled ignition to be homogeneously distributed over the fire domain, hence $\rho_i = \frac{1}{I}$. Fig. 4 illustrates the overall domain of study along with the ignition locations and the candidate sensor locations. Table 1 summarizes the geographical information that specifies the area of study and the discretization parameters used here.

The typical detection distances for current sensor technology for EWDS range from 10 to 100 m (Mohapatra and Trinh, 2022). Given the raster spatial resolution (see Table 1), this range is in agreement with the assumption that sensors respond accurately as soon as their trigger (e.g., fire, particle concentration, heat, sound, etc.) reaches the cell in which they are located.

The candidate sensor location and the ignition grids both share the same resolution but are shifted to avoid overlapping and spurious fire detections. The resolution of the simulated raster datasets limits the density of the grids of the ignitions and candidate sensor locations. In

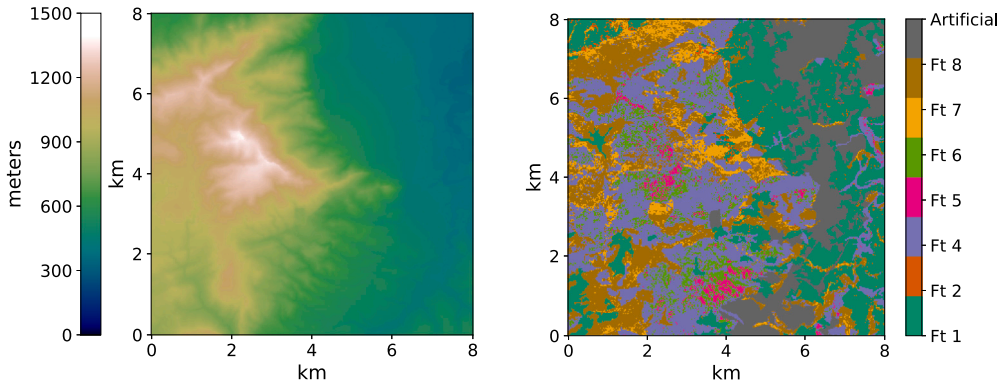


**Fig. 3.** Left, elevation map from the study area. Right, Rothermel fuel types (Ft) computed in Gómez-González et al. (2024). The legend corresponds to the specification given in Anderson (1982), Short Grass (Ft 1), Timber Grass and Understory (Ft 2), Chaparral (Ft 4), Brush (Ft 5), Dormant Brush (Ft 6), Southern Rough (Ft 7), Compact Timber Litter (Ft 8). Artificial: Urban and Industrial areas.

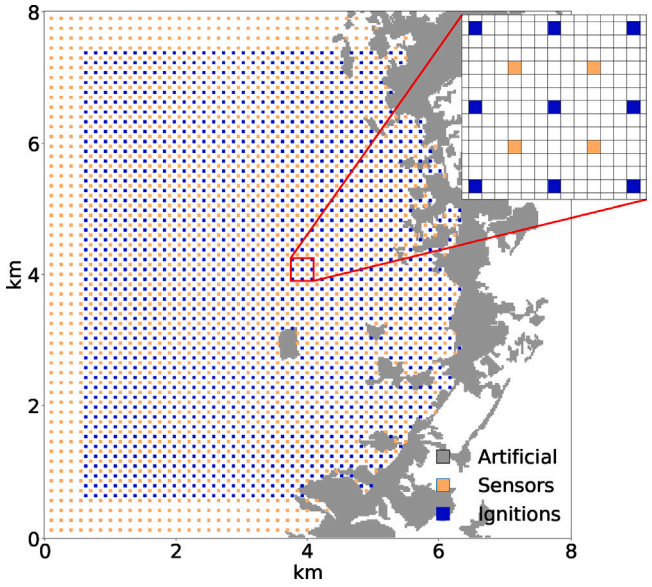


**Fig. 4.** Fire domain with grids defining candidate sensor and ignition locations considered in this study. Areas in grey colour represent urban and industrial areas. The inset plot offers a close-up view of both grids.

**Table 1**
Geographical parameters of the fire domain, the lattice discretization, and spatial coordinates for the ERA5 weather reanalysis and Fire Weather Index (FWI) data retrieval.

| Geographical parameter | Value |
|---|---|
| Number of cells in x-axis ($L_x$) | 321 |
| Number of cells in y-axis ($L_y$) | 321 |
| South-West corner x | 715 987.5 m (ETRS89, zone 31N) |
| South-West corner y | 4 287 987.5 m (ETRS89, zone 31N) |
| Cell size in x-axis ($C_x$) | 25 m |
| Cell size in y-axis ($C_y$) | 25 m |
| Total area | 6441 ha |
| Area covered by sensors | 4541 ha |
| ERA5 coordinate x | 713 658.213 m (ETRS89, zone 31N) |
| ERA5 coordinate y | 4 296 347.495 m (ETRS89, zone 31N) |
| FWI coordinate x | 717 405.761 m (ETRS89, zone 31N) |
| FWI coordinate y | 4 286 452.733 m (ETRS89, zone 31N) |

the case study considered here, we have 65,760 flammable cells, so this is also the maximum number of ignition and candidate sensor locations. Ignition locations and candidate sensor locations are arranged uniformly to ensure an unbiased exploration and monitoring of fire dynamics across the different geographical zones.

**Table 2**
Resolution $\delta$, boundary offset $\lambda$, and number of cell candidates for ignition and sensors parameters.

| Grid parameter | Candidate sensor locations | Ignitions |
|---|---|---|
| Cell candidates ($n_{candidates}$) | 2650 | 2300 |
| Final valid cells | 1961 | 1556 |
| Cell separation ($\delta$) | 5 | 5 |
| Grid offset ($\lambda$) | 4 | 25 |

Ignitions are not distributed close to the boundaries of the grid to avoid inaccurate fire simulations due to the finite size of the domain. Sensor placements, on the contrary, extend to the boundaries of the grid to allow the detection of fires spreading in all directions.

The grid specification takes into account that raster cells categorized as non-wildland fuels are not suitable for ignition, nor as candidate sensor locations (see Fig. 4). The grids of ignition locations $\vec{r}_i$ and candidate sensor locations $\vec{r}_l$ are defined following the procedure shown in algorithm 2. The result is a squared lattice of cells, spaced $\delta$ cells apart, among adjacent locations of ignitions and candidate sensors, offset $\lambda$ cells from the boundary of the domain. Table 2 summarizes the parameters that define the grids of ignitions and candidate sensor locations.

**Algorithm 2** Definition of ignitions and candidate sensor locations. The operators $\lfloor\bullet\rfloor$ and $\lceil\bullet\rceil$ denote the floor and ceiling functions, respectively. The values of the parameters are found in Tables 1 and 2.

$\eta \leftarrow \lceil \frac{L_x-\lambda}{(\delta+1)} \rceil$, number of candidates in x-axis
**for** $z = 1, n_{candidates}$ **do**
  $x_z \leftarrow \frac{C_x}{2}\left((z-1)(\delta+1)+\lambda-\eta\delta\lfloor\frac{(z-1)}{\eta}\rfloor\right)$
  $y_z \leftarrow \frac{C_y}{2}\left(\lambda+(\delta+1)\lfloor\frac{(z-1)}{\eta}\rfloor\right)$
  **if** $Fuel(x_z, y_z) \neq$ "Artificial" **and** $\vec{r}_z$ is "Left Cocentaina" **then**
    $\vec{r}_z \leftarrow [x_z, y_z]$
  **end if**
**end for**

### 3.4. Fire-weather scenarios

This study aims to optimize the WSN performance to operate during high-danger fire-weather conditions when the likelihood of severe fire is higher. The meteorological information used in our research is the ERA5 weather reanalysis dataset (Copernicus Climate Change Service (C3S), 2018), provided by the European Centre for Medium-Range Weather Forecasts (ECMWF). To assess fire danger, our study implements the fire danger forecast based on the Canadian Forest

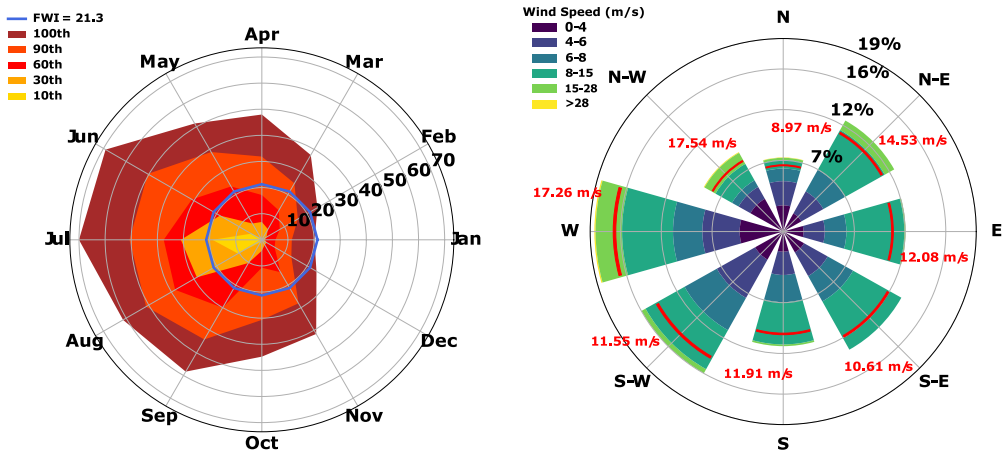


**Fig. 5.** Left, Percentile distribution of Fire Weather Index (FWI) data by month with the concentric blue line noting days with high-danger fire-weather conditions. Right, the wind rose, summarizing the wind distribution during days with high-danger fire-weather conditions. Red concentric sections, with numbers, indicate the 90th wind speed percentile. (For interpretation of the references to colour in this figure legend, the reader is referred to the web version of this article.)

**Table 3**
Wind speeds and direction statistics used for the optimization.

| Wind direction | 90th percentile of wind speed (m/s) | Frequency $\omega_j$ |
|---|---|---|
| North | 8.97 | 7.30% |
| North-East | 14.53 | 12.52% |
| East | 12.08 | 12.04% |
| South-East | 10.06 | 13.33% |
| South | 11.91 | 11.27% |
| South-West | 11.55 | 15.99% |
| West | 17.26 | 18.59% |
| North-West | 17.54 | 8.96% |

Fire Weather Index (FWI) System provided by ECMWF (Copernicus Emergency Management Service (CEMS), 2019). We consider historical data 5 years before the fire incident of Cocentaina in 2012 because meteorology after a wildfire is potentially affected at the local and regional scale (Hantson et al., 2022). Table 1 summarizes the geographical coordinates where this data is referred to, and Fig. 5 shows the FWI and wind distribution data.

FWI values greater than 21.3 correspond to days with high-danger fire-weather conditions according to the European Forest Fire Information System (EFFIS) (2007) classification (Concentric blue line in Fig. 5-left). Consequently, our study omits meteorological information from days with smaller FWI values.

The main weather magnitudes affecting fire behaviour used in the model are fuel moisture and winds (Gómez-González et al., 2024). On the day of the fire event, the FWI value was 37, ranking as the 87th percentile in the dataset. Therefore, we consider that fuel moisture values computed in the previous study are representative of the high-danger fire-weather conditions in which the WSN is expected to operate, and no other scenario is considered.

The wind rose in Fig. 5-right, shows the distribution of winds across the eight cardinal directions during high-danger fire-weather days, with the radial scale indicating wind frequency per direction and the shades of colour showing the distribution of wind speeds. For each wind direction, we estimate the 90th percentile wind speed as the expected worst-case scenario (concentric red sections in Fig. 5-right). Following the Beaufort scale (Encyclopaedia Britannica, 2024), their intensities range from class 5 (fresh breeze) to 7 (high wind). The fire-weather frequency coefficients $\omega_j$ are determined by the frequency of wind directions. These wind values, tabulated in Table 3, are the inputs to the simulator WindNinja (Wagenbrenner et al., 2016) to generate the wind fields. Fig. 2 showcases the wind fields corresponding to the North-West and East winds.

## 4. Results

This section introduces the optimization results for the Cocentaina case study (Section 3) according to the formulation of Section 2.5 and the wind frequencies of Section 3.4. Then, the performance of networks is compared with the following three cases:

- The no-sensors case using Free-Spreading Fires (FSF) burnt area statistics after 1/2 h, 1 h, and 3/2 h.
- Uniform WSN cases without optimization.
- Fixed-weather cases using networks optimized for each scenario.

The uniform WSN cases are defined over the same set of candidate sensor locations as the solution space $\Omega$. Sensors are placed at a distance of $\upsilon$ metres, following a squared symmetrical pattern. When $\upsilon$ decreases, the network size increases. For the same $\upsilon$, we can define more than one WSN due to the possibility of sliding the lattices over the grid of candidate sensor locations. We consider the ensemble of all uniform lattices for each $\upsilon$ $\mathbf{U}_{[\min(f_2),\max(f_2)]}(\upsilon) = \{\vec{u}_\upsilon^1, \vec{u}_\upsilon^2, \dots, \vec{u}_\upsilon^{N_\upsilon}\}$. $N_\upsilon$ stands for the number of lattices with $\upsilon \in V$, being $V$ the set of distances. This study presents uniform networks for $V = \{300, 450, 600, 750, 900\}$ metres. For the remainder of the study, we will refer to the uniform lattices by their number of sensors. For instance, Fig. 8-centre displays the $\mathbf{U}_{204}$ WSN, including 204 sensors, for $\upsilon = 450$ m. The comparison outcomes are also analysed, with a closer examination of their implications, in Section 5.

### 4.1. Optimized WSN localizations

The optimizer parameters used in the study are presented in Table 4. In NSGA-II, the population size, the offspring population, and the number of generations control the speed and the quality of the model convergence. Given the numbers in Table 4, the optimization runs involve the assessment of nearly 8,000,000 alternative WSNs — evaluated as population size + (number of generations × offspring population). These parameters can be linked to the size of the solution space and the desired resolution of the Pareto front approximation, as explained below. The crossover and mutation probabilities use the default values from Pymoo. The population sizes and the number of generations are sufficiently large to ensure convergence and to adequately cover the Pareto front. Convergence was confirmed by observing the improvement of the front between successive generations. The choice for a larger population size in the unconstrained case is to maintain the same resolution in the results since the Pareto front is wider for the unconstrained problem. Note that if we applied

**Table 4**
Values of optimizer parameters for optimization runs without/with the DBA constraint.

| Parameter | Without constraint | With constraint |
|---|---|---|
| Population sizes | 300 | 150 |
| Offspring population | 20 | 20 |
| Number of generations | 400,000 | 400,000 |
| Number of WSN assessments | 8,000,300 | 8,000,150 |

**Table 5**
Performance statistics for constrained ($\vec{s}_{f_2}(g)$) solutions. Data reported for the solution with the fewest sensors under each constraint.

| Solution | | DBA (ha) | | |
|---|---|---|---|---|
| $\vec{s}_{f_2}(g)$ | $f_1$ | 50th | 90th | 95th |
| $\vec{s}_{407}(10)$ | 2.92 | 2.69 | 6.56 | 7.69 |
| $\vec{s}_{350}(12)$ | 3.23 | 3.00 | 7.19 | 8.38 |
| $\vec{s}_{293}(15)$ | 3.81 | 3.75 | 8.56 | 10.19 |
| $\vec{s}_{232}(18)$ | 4.97 | 4.69 | 10.81 | 12.56 |
| $\vec{s}_{173}(25)$ | 6.28 | 5.56 | 14.00 | 16.62 |
| $\vec{s}_{155}(30)$ | 7.04 | 6.25 | 16.25 | 19.06 |
| $\vec{s}_{119}(40)$ | 8.91 | 8.12 | 21.44 | 25.50 |
| $\vec{s}_{96}(50)$ | 10.96 | 9.69 | 26.25 | 31.06 |
| $\vec{s}_{70}(60)$ | 14.51 | 13.31 | 33.19 | 39.31 |
| $\vec{s}_{58}(90)$ | 17.41 | 16.56 | 40.12 | 49.12 |
| $\vec{s}_{46}(110)$ | 21.58 | 20.16 | 51.94 | 63.00 |

**Table 6**
Best performing uniform grids for each $\upsilon$, DBA performance statistics, and the loss in performance compared to $\vec{s}_{f_2}(\sim)$ with the closest $f_2$ value — evaluated as $100 \times [f_1(\mathbf{U}_{f_2}) - f_1(\vec{s}_{f_2}(\sim))]/f_1(\mathbf{U}_{f_2})\%$.

| Solution | | | DBA (ha) | | | $\Delta f_1$ (%) |
|---|---|---|---|---|---|---|
| $\upsilon$ (m) | $\mathbf{U}_{f_2}$ | $f_1$ | 50th | 90th | 95th | |
| 300 | $\mathbf{U}_{472}$ | 4.52 | 4.12 | 9.38 | 11.56 | 77.20 |
| 450 | $\mathbf{U}_{210}$ | 10.22 | 8.81 | 20.94 | 26.50 | 99.61 |
| 600 | $\mathbf{U}_{123}$ | 17.24 | 15.75 | 36.12 | 43.25 | 110.64 |
| 750 | $\mathbf{U}_{81}$ | 26.15 | 25.00 | 54.56 | 61.88 | 113.35 |
| 900 | $\mathbf{U}_{50}$ | 35.87 | 35.12 | 82.50 | 95.38 | 80.04 |

exhaustive enumeration, we would need to assess $4 \times 10^{227}$ alternative networks only for a fixed size of 150 sensors. The final set of non-dominated solutions generated by each run approximates the Pareto fronts. Although it cannot be proven analytically that these solutions match the exact optima, for reasons of simplicity, we use the term "optimal" in the remaining text for the set of solutions obtained here. Optimization experiments are performed for different scenarios of constraint values, summarized in Table 5, where the obtained optimal WSNs are denoted by $\vec{s}_{f_2}(g)$. The optimal scenario without constraint is computed as well, using the notation $\vec{s}_{f_2}(\sim)$ when discussing their WSNs through the results and discussion.

### 4.2. Comparison of optimal WSNs to uniform grids

The optimizer proposes designs that significantly outperform the uniform networks of similar size, in terms of DBA and detection times. Table 6 presents statistics of the best performing $\mathbf{U}_{f_2}$ solutions for each $\upsilon$. The column $\Delta f_1(\%)$ indicates the percentage increment of $f_1$ compared to the values from the $\vec{s}_{f_2}(\sim)$ networks (i.e. unconstrained solutions) closest in size — evaluated as $100 \times [f_1(\mathbf{U}_{f_2}) - f_1(\vec{s}_{f_2}(\sim))]/f_1(\mathbf{U}_{f_2})\%$. The best performing uniform cases present $f_1$ values 77% to 113% larger than the same size $\vec{s}_{f_2}(g)$ across all $\upsilon$ separations.

Fig. 6a illustrates the $\vec{s}_{f_2}(\sim)$ WSNs in small grey dots, defining their estimated Pareto-front. Likewise, $\vec{s}_{f_2}(g)$ WSNs are shown as orange circles with their constraint values indicated atop their markers (in units of ha). These constrained solutions showcase the smallest networks found in their estimated Pareto-fronts, presented in Table 5, along with several DBA statistics. Fig. 6b presents the previous optimal WSNs correlating their number of sensors with the average fire detection times. The average detection time of an optimal WSN is computed by aggregating the detection times $t_{i,j}^{\text{detection}}(\vec{s})$ of every simulated wildfire by their ignition likelihood and the frequency of winds. Fig. 6a–b include the evaluation of $f_1$ and $f_2$ for the uniform cases as well.

Fig. 6a–b show the performance of $\mathbf{U}_{[\min(f_2),\max(f_2)]}(\upsilon)$ compared to that of the optimal WSNs. The range of sensors characterizing each ensemble of uniform grids is indicated in brackets as $[\min(f_2), \max(f_2)]$, with $\upsilon = 300$ m corresponding to the densest configurations and $\upsilon = 900$ m to the less dense configurations. $\mathbf{U}_{f_2}$ exhibit performance variability due to the different spatial arrangements for a given $\upsilon$. The horizontal bars present the range between the minimum and maximum $f_1$ (Fig. 6a) and average time values (Fig. 6b); the vertical bar displays the WNS size range, with the minimum and maximum $f_2$ values. The vertical and horizontal bars cross at the median on $f_1$ and the average detection time. The variability in performance, both the average time detection and DBA gaps, reduces with increasing WSN size. However, this pattern can be influenced by the maximum sensor density determined by the resolution of the candidate sensor grid, leading to greater variability reduction than reality. (see Section 5.2 for discussion).

**Table 7**
Free-spreading fire (FSF) simulations BA statistics after different times.

| Time (h) | Mean (ha) | 50th (ha) | 90th (ha) | 95th (ha) |
|---|---|---|---|---|
| 1/2 h | 3.21 | 2.31 | 7.62 | 9.44 |
| 1 h | 11.42 | 8.62 | 26.58 | 32.12 |
| 3/2 h | 23.71 | 18.62 | 54.25 | 64.73 |
| 5 h | 234.38 | 237.19 | 434.66 | 487.74 |

### 4.3. Detected burnt area distribution analysis

Table 7 presents several statistics of FSF after 1/2 h, 1 h, 3/2 h, and the final simulation time of 5 h (Table 5). The comparison of Tables 5 and 7 shows that for optimal networks with $f_2 \geq 119$, detected fire sizes are consistently smaller than the FSF benchmark over 1 h. However, Fig. 6b indicates that the average detection time for 119 sensors is approximately 1,1 h, suggesting a proportion of fires are detected later than 1 h. This result highlights how the methodology targets fast-spreading fires—those in the upper FSF percentiles — while slower-spreading fires tend to be detected later.

Fig. 7 uses box plots to compare the dispersion of DBA for a series of optimal WSNs (in orange) with increasing size and two particular cases of uniform networks (in blue) with inter-sensor separations $\upsilon = 300, 450$ m, $U_{479}$, $U_{204}$ respectively. The box plots highlight the interquartile range, with the graphical box enclosing the 25th and 75th percentiles. The line inside the box indicates the median of the dataset. For this particular representation, whiskers outside the interquartile range denote the 5th and 95th percentiles. Values outside the 5th–95th range are considered outliers and plotted individually. Vertical lines highlight the 95th percentile of FSF BA after 1 h, 1/2 h, and 3/2 h. Since these represent high FSF percentiles, detected burnt areas below these values suggest the involved network triggers dangerous fires before they freely spread beyond those time marks.

For $\vec{s}_{155}(30)$, 75% of fires are detected at sizes smaller than the 95th percentile of free spreading at 1/2 h. In contrast, for $\mathbf{U}_{204}$, most outliers exceed the 95th percentile at 1 h, extending up to the 95th percentile at 3/2 h. This limitation leaves many dangerous fires undetected for over 1 h, far exceeding the 30 ha threshold. Correspondingly, as more sensors integrate the network from the same optimal Pareto (30 ha restriction), the DBA improves, with no outliers spreading above 95% of BA for 1 h.

For optimal WSNs the 75th DBA percentiles are smaller than the 50th DBA percentiles observed in $\mathbf{U}_{204}$ and only outliers exceed the 75th percentile of detections in $\mathbf{U}_{204}$, even with a comparable number of sensors. To achieve similar performance with $\mathbf{U}_{f_2}$ lattices, a denser configuration with $\upsilon = 300$ metres is required, as demonstrated by

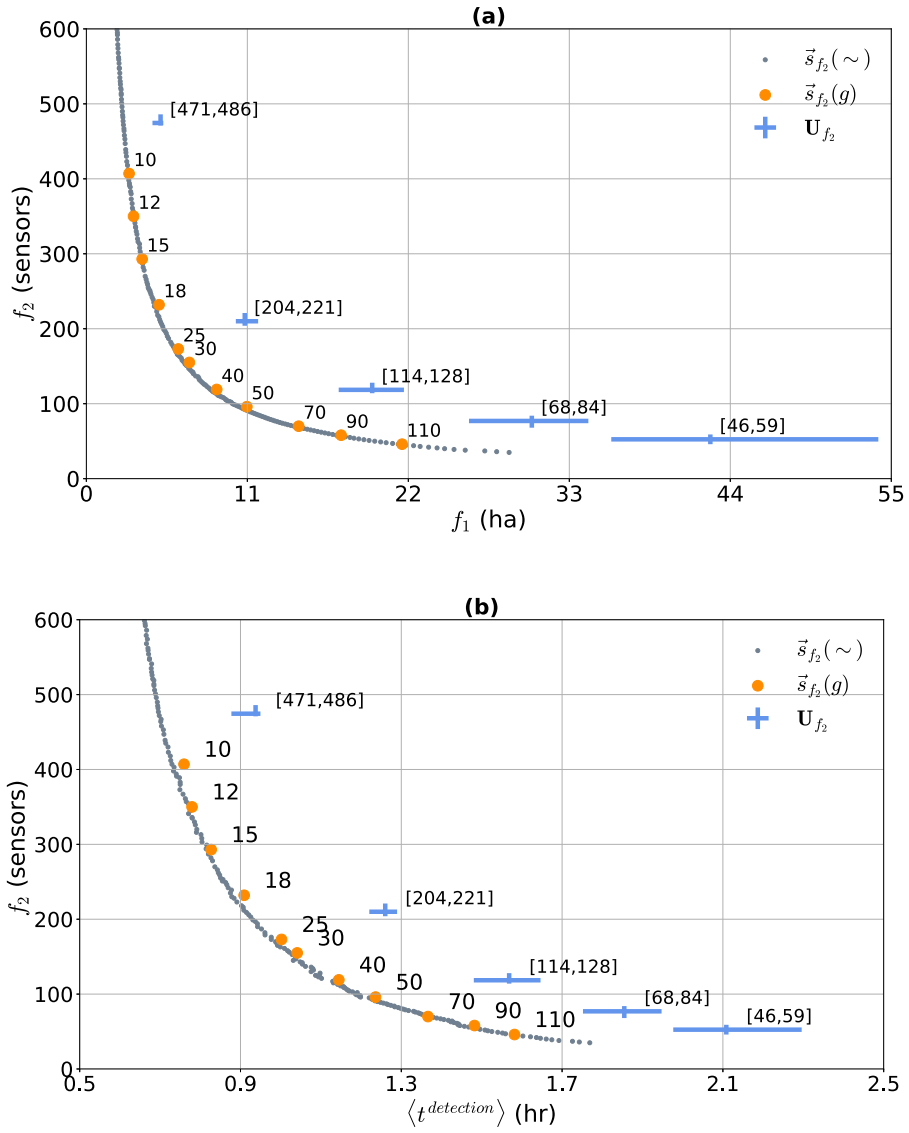


**Fig. 6.** All-winds optimization results. Markers ● represent constrained optimal solutions, ● unconstrained optimal solutions, and for the uniform grids, ▬ cover the min–max performance and ▮ the min–max number of sensors. (a, top): WSN size (number of sensors, $f_2$) versus the Detected Burnt Area (DBA) objective ($f_1$), defining the unconstrained Pareto. (b, bottom): WSN size (number of sensors, $f_2$) versus the average detection time. (For interpretation of the references to colour in this figure legend, the reader is referred to the web version of this article.)

the 479-sensor example, requiring a 123% increase in sensor count compared to $\vec{s}_{215}(30)$. While uniform grid detections show large DBA dispersion, optimal DBA distributions are better bounded, with outliers remaining below 30 ha. The constraint ensures no outliers exceed this value, offering an operational mechanism for detecting fires within a specified size limit.

### 4.4. Landscape Burnt Probability Map (LBPM)

The Landscape Burnt Probability Map (LBPM) is a standard metric used to evaluate fire susceptibility (Argañaraz et al., 2017). We use the set of wildfire simulations across ignitions $I$ and weather scenarios $K$ to compute the frequency of times cells burn. Then, the LBPM is the normalized frequency, constituting a probability estimate. Fig. 8 presents the LBPM without sensors progressing up to the final simulation time of 5 h and with the adoption of WSNs. For illustrative purposes, we consider a 30 ha constraint for the optimal WSN, aiming to use the fewest sensors possible to minimize finite resolution effects. The network $\vec{s}_{155}(30)$ has the fewest number of sensors; however, it is not feasible to arrange a uniform grid with 155 sensors within this area. Therefore, we examine the closest alternative of size $\mathbf{U}_{204}$, utilizing $\vec{s}_{204}(30)$ for a fair comparison.

Fig. 8 compares the LBPM with the different scenarios sharing the same logarithmic scale. Note that the LBPM is computed at fire detection in the presence of sensors. In reality, we would expect a larger burnt likelihood since the fire will continue after detection until it is suppressed. However, our results concentrate on the detection phase and aim to improve detection time and reduce the burnt area before detection. Clearly, this would also improve response mechanisms, though they are not considered in the present work.

With the optimal WSN, it results in a homogeneous distribution of values across the domain with an average DBA, $f_1$, of approximately 5 ha (Fig. 6a), 48 times lower than the BA obtained with no-sensors after 5 h. Fig. 8 also highlights four different sub-regions delimited by dashed (a and b) and dotted (c and d) rectangles. The dashed rectangles a and b designate areas with naturally low LBPM. The optimizer avoids placing sensors within these areas and instead favours candidate locations along their borders, prioritizing coverage of other regions using the sensor surplus. The dotted rectangles c and d indicate areas that are narrowly connected to the main domain, in which no ignitions were

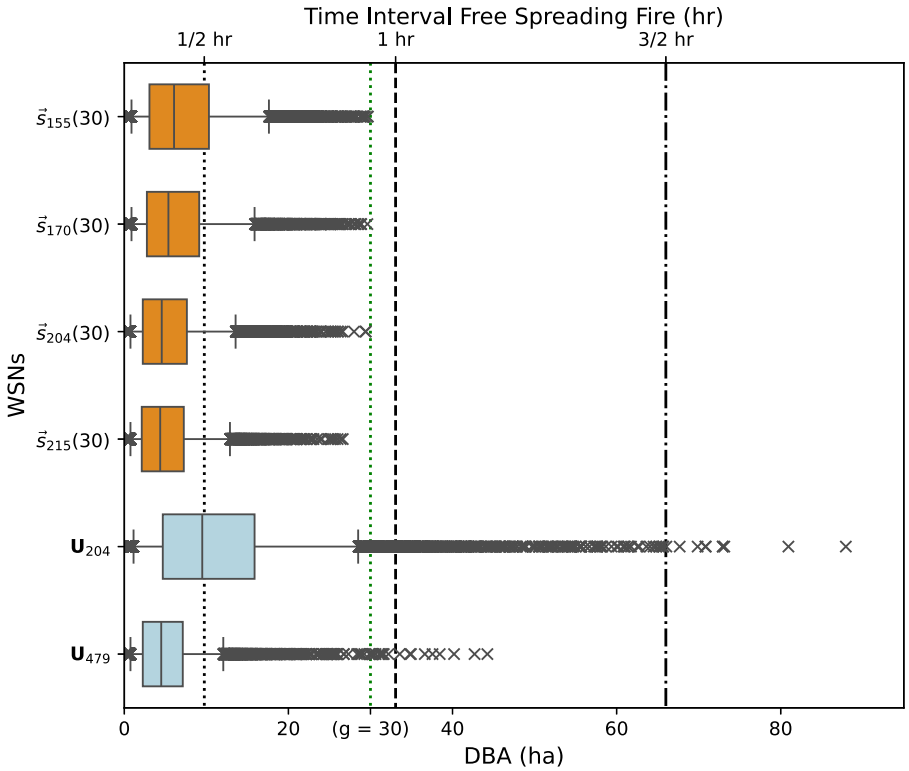


**Fig. 7.** Box plot representation of DBA (including 12488 simulations each) distributions for optimal (orange) and uniform WSNs (blue) (bottom x-axis). Vertical lines denote the 95th BA free-spreading fires (FSF) percentiles at different times (top x-axis). Note how, by design, the optimal sensors locations prevent large-size fires with the 30 ha constraint (vertical green line), unlike the uniformly distributed WSNs. (For interpretation of the references to colour in this figure legend, the reader is referred to the web version of this article.)

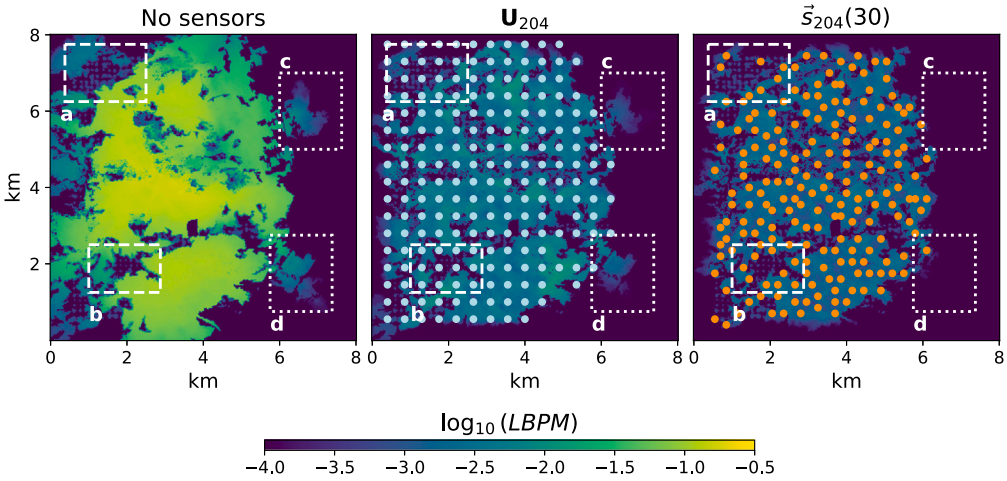


**Fig. 8.** Landscape Burnt Probability Map (LBPM): without sensors (left), with a uniform grid with 204 sensors ($\mathbf{U}_{204}$, centre), and with the optimal solution with 204 sensors ($\vec{s}_{204}(30)$, right). The optimal WSN autonomously avoids monitoring areas with low fire susceptibility (a, b) and identifies fire corridors (c, d), detecting fires spreading across the urban area.

considered (see Fig. 4) but where fire is able to spread, compromising the WUI further. The optimal solution $\vec{s}_{204}(30)$ protects these domains by effectively reducing to zero the LBPM. For further examination, Table 8 presents the statistics for the no-sensors, uniform, and optimal scenarios.

In order to assess how the LDPM improves when a WSN is used, we compare the decrease in the LBPM's median as follows: $100 \times [50th(\text{no-sensors}) - 50th(WSN)]/50th(WSN)\%$. The $\mathbf{U}_{204}$ configuration offers a large improvement in the LBPM of a 1500% decrease in the median value with the no-sensors case. Nevertheless, the optimal configuration provides a 2700% improvement with respect to the

**Table 8**
Landscape Burnt Probability Map (LBPM) statistics for different scenarios. The last column shows the percentage reduction in the median LBPM value relative to the WSN scenarios, computed as $100 \times [50th(\text{no-sensors}) - 50th(WSN)]/50th(WSN)\%$.

| Scenario | $\log_{10}$(50th) | $\log_{10}$(90th) | $\log_{10}$(95th) | $\log_{10}$(max) | Δ 50th |
|---|---|---|---|---|---|
| No sensors | −1.32 | −0.91 | −0.84 | −0.74 | – |
| $\mathbf{U}_{204}$ | −2.52 | −2.21 | −2.12 | −1.87 | 1479% |
| $\vec{s}_{204}(30)$ | −2.77 | −2.54 | −2.48 | −2.07 | 2665% |

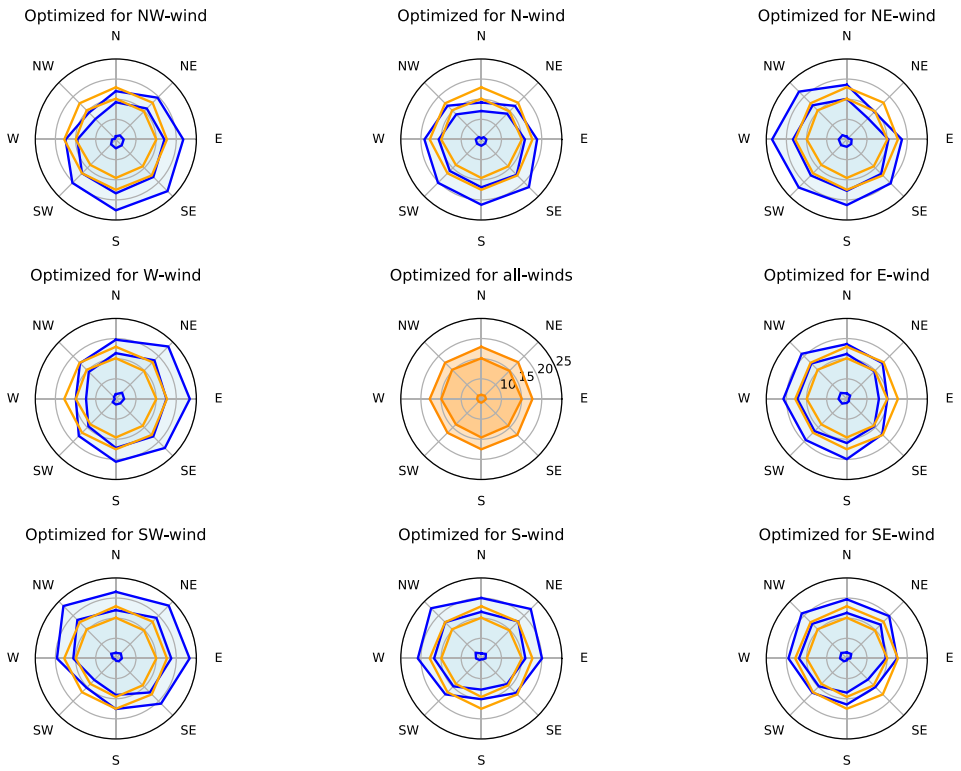


**Fig. 9.** DBA statistics assuming the 8 single-wind optimal WSNs (blue lines) and the all-wind WSN (orange lines). In all instances, the constraint is DBA < 30 ha and the size of 155 sensors. Each polar plot shows the median, 90th and 95th DBA percentiles for fires in different wind directions. For detailed wind data, see Table 3. (For interpretation of the references to colour in this figure legend, the reader is referred to the web version of this article.)

no-sensors scenario, approximately doubling the improvement with respect to the uniform network. In addition, uniform networks do not re-adapt to regions with already low LBPM values, invest in unnecessary sensors, and cannot prevent fires from spreading through narrow fire corridors, leading to unexpected damage.

### 4.5. Comparison of optimal WSNs with networks optimized for fixed-weather cases

In this section we analyse the variability in performance when we optimize for fixed wind directions. Following the wind rose in Fig. 5, we consider eight independent pairs of wind directions and speeds. We obtain the optimal WSN for each pair by limiting the WSN optimization to the relevant simulations. In all cases, we also apply the constraint of 30 ha to the maximum burnt area. For the comparison, we consider the fixed-wind optimal WSNs comprising 155 sensors and compare their performance against the $\vec{s}_{155}(30)$ WSN presented in Section 4.1.

Fig. 9 shows the performance of optimal networks obtained with all-wind conditions in orange and those optimized for each wind component in blue. The visualization presents the median, 90th and 95th DBA distribution percentiles in polar coordinates. Each polar plot shows the statistics on the radial dimension, with values ranging from 0 to 25 ha. The fixed-weather WSNs only outperform the $\vec{s}_{155}(30)$ in detecting the subset of fires for which they were optimized, as the statistics are lower for those specific wind directions. When the fire data correspond to adjacent wind directions, the fixed-weather WSNs perform similarly well to the all-winds optimal configuration, but the performance systematically worsens as the winds veer, with the worst performance for the opposite direction. On the contrary, $\vec{s}_{155}(30)$ detects fire evenly across the wind rose directions despite the variability in the frequency and intensity of winds. Similarly to the LBPM metric, including wind uncertainty information during the optimization of sensor locations homogenizes the performance across the scenarios considered.

## 5. Discussion

### 5.1. Analysis of scope

The results highlight the quantitative benefits of having an optimal WSN compared to using uniform networks and, as expected, not having any WSN at all. We discuss here specific solutions, such as those with 155 or 204 sensors, to facilitate the comparisons and the discussion. It is up to the stakeholders to determine which one of the final solutions from Fig. 6a best meets their specific requirements. However, the final decision on which solution to implement is outside the scope of this work, and may also consider issues such as the sensor redundancy, the WSN cost, the total available budget, the detection accuracy, etc.

For the no-sensors case, improvements are analysed with respect to the BA of **free-spreading wildfires (FSF)** at different times. Complex wildfire dynamics leads to an accelerating increase of burnt area as time passes, hampering the scenario with successful fire suppression. Optimal WSNs allow the detection of fires, including the most dangerous ones, before 1 h and a large proportion even before 1/2 h. In contrast, for similar sensor counts, uniform networks detect dangerous fires later than 1 h and even after 3/2 h, requiring more than twice as many sensors to match optimal performance. The case study comprises 41 km$^2$, thus demonstrating the practicality of this optimization framework in extensive domains.

Using **uniform WSNs** is a common approach; it is straightforward and constrained by budget. However, the fact is that optimal WSNs outperform uniform networks of similar sizes regarding the average DBA and its distribution (illustrated by computing the median, 90th percentile, and 95th percentile). Dynamic data allows placing sensors in anticipation of fire spread, facilitating collaboration in the detection. It is also observed that the predictability of uniform networks is less robust since their performance for the same size depends heavily on the exact location of the first sensor. Inspecting the performance ranges of uniform grids in Fig. 6a–b, for the $\mathbf{U}_{204}$-$\mathbf{U}_{221}$ WSNs, the average DBA

ranges between 10 and 12 ha, and the average detection time between 72 and 78 min. Meanwhile, the closest $f_2$ optimal WSN exhibits $f_1$ = 5 ha (a reduction of 100%–140%) and an average detection time of 54 min (a reduction from 25%–31%). According to Table 6, the improvement of the optimal $\vec{s}_{f_2}(\sim)$ WSNs over their closest in size best-performing $\mathbf{U}_{f_2}$ WSNs goes from 77% to 113% across all sensor-to-sensor distances $v$. In addition, with optimal WSNs, fire susceptibility is reduced evenly across the landscape (see Fig. 8), demonstrating better mitigation of all fire cases, showcasing a 80% improvement in the most common value compared to the uniform grids as well (see Table 8), which for other statistics can be observed to increment up to 100%. All our indicators suggest an approximate 100% improvement with respect to the uniform approach across different sensor spatial densities indicated by $v$.

Although the average DBA ($f_1$) specifies the overall performance, the shape of the distribution provides information about the largest fires escaping detection. In Fig. 7, we use box plots to study the DBA dispersion. As expected, when we apply the 30 ha constraint on the DBA size, none of the fires exceed this bound upon detection. Generally, the optimal DBA statistics are well below the constraint, with only some outliers approaching the operational fire limit size. On the contrary, for the $\mathbf{U}_{204}$ WSN, most of the outliers escape the operational limit of 30 ha and the $\mathbf{U}_{479}$ WSN still presents a small number of outliers despite its size. With less than half of the sensors, $\vec{s}_{155}(30)$ DBA distribution is similar without fires escaping to unmanageable sizes.

### 5.2. Analysis of trade-offs

The results of Section 4.1 allow us to study the **trade-offs between the size of the all-wind optimized WSNs and their performance**. The Pareto front in Fig. 6 spreads from 35 sensors to 600 sensors, although the full set of solutions produced by the optimization ranges up to 1200 sensors. However, it is not practical to have extremely large (too expensive) or extremely small WSNs (ineffective in detecting fires). Below 40 sensors, a small decrease in the network size leads to a significant increase in average DBAs (approximately 1 ha per sensor). The time also increases by 1 min per sensor. Above 200 sensors, we need to invest significantly to achieve a small benefit in terms of the DBAs (14 sensors to reduce the average DBA by 1 ha) and the detection time (>17 sensors per minute). Note that, as the WSN size reaches the maximum allowable of 1961 sensors, the average DBA converges to approximately 3 ha because of the finite resolution of the grid of candidate sensor locations. Assuming isotropic propagation, the wildfire attribute, which in our case study corresponds to the fire perimeter, spreads approximately 50 cells (3 ha) before crossing the nearest candidate sensor locations (See Fig. 4).

We can also use the optimizer to introduce constraints and study the effect of other performance preferences on the obtained WSNs. As we introduce the DBA constraints, we observe in Fig. 6a that the constrained Pareto fronts nearly match the unconstrained front (with minimal deviation in terms of performance), but starting from a larger WSN size as the constraint value increases. For the limit of 30 ha, an indicator of a higher fire severity index as estimated in Gobierno de Castilla y León (1999), the minimum number of sensors is 155 in this landscape.

### 5.3. Analysis of robustness

In Section 4.5, we prove the **importance of considering all possible weather conditions** instead of a single scenario. When we optimize for fixed-wind conditions, the obtained WSNs demonstrate competitive performance in detecting fires spreading for adjacent wind directions. This result is expected since the spread of fire should not diverge much in similar wind directions. However, the performance greatly diminishes as the wind shifts more. Despite the detection distributions from fixed-wind WSNs and the $\vec{s}_{155}(30)$ converging for smaller fires (as shown by the similarity in the median values in Fig. 9), the marginal gain in a single direction does not offset the performance degradation across other wind conditions. So, this analysis confirms the importance of considering variable weather scenarios during the optimization to generalize effectively across different fire conditions. Note that the fixed-wind runs use fewer fire data, and the assessment of each alternative WSN is less computationally demanding. However, the optimization search uses the same number of generations and population size.

Looking at the wind statistics (Table 3), the higher frequency of West (18.59%) and South-West (15.99%) directions indicate that these are scenarios with higher risk than others. However, it is important to mention that the 2012 wildfire, which burned 546 ha in Concentaina, initiated and evolved during its initial stages under East and South-East wind conditions (Gómez-González et al., 2024). Therefore, a WSN optimized only for West or South-West winds may compromise the detection of potentially disastrous ignitions.

The LBMP analysis shows that the $\vec{s}_{204}(30)$ configuration evenly reduces fire susceptibility across the fire domain, avoiding the placement of sensors in areas where fire spread is not dangerous. Moreover, it can identify fire pathways, while the uniform configuration completely ignores them.

The computational effort for each assessment scales linearly with the number of fire scenarios and candidate sensor locations. Due to the combinatorial nature of our optimization problem, which resembles a 0–1 knapsack problem (Jaszkiewicz, 2004), the convergence increases exponentially with the number of candidate sensor locations. When the problem size becomes challenging, a solution can be proposed that involves partitioning the domain. However, this method may lead to numerical issues that require further evaluation.

## 6. Conclusions

In this work, we develop and implement a decision support tool for the strategic deployment of Wireless Sensor Networks (WSNs) as an Early Wildfire Detection System (EWDS) with the potential to enhance subsequent fire suppression phases. It follows a multi-objective optimization approach, and it is able to accommodate (a) datasets from different simulators, (b) biases on the ignition locations or conditions, and (c) inputs from different data, such as varying weather conditions or changes in fuel distribution. In addition, the problem formulation can consider different objective functions or constraints. Thus, the study provides an example to demonstrate the capacities of the optimizer. If there is information on firefighting resources or road networks, WUI/WII mapping, we can modify the problem formulation (i.e. use additional constraints or introduce biases on specific areas) to alter the trade-offs and prioritize sensor placement in areas where they would most effectively support firefighting efforts.

Results are obtained for a well-studied region in South-East Spain, demonstrating the capabilities, efficiency and robustness of the proposed framework. Our choice highlights the relevance of having accurate and diverse data (fuel, weather conditions, topography…) and a simulator that can accommodate those pieces of information with a small computational cost. We consider only the effect of wind conditions as the governing factor driving wildfire spread to provide a proof of concept of the proposed optimization approach. This methodology allows the exploitation of more complex weather scenarios, depending on the requirements of the specific application.

For this region, we use a practical implementation of the optimizer to minimize the average detected burnt area (as the detection performance estimator) and the number of sensors (as an estimator of the network cost) and explore a range of constraints to satisfy operational demands. The proposed problem formulation accommodates the stochasticity of fire conditions so that the optimal WSN configurations perform equally well over the entire range of expected

scenarios. Comparisons with WSNs optimized for single meteorological scenarios confirm the critical role of considering the diversity of weather conditions in the optimization process and the robustness of the proposed formulation. The optimal networks are also compared to non-optimized uniform networks, a usual practice in WSN design. The statistical analysis reveals significant improvements in the performance of optimal WSNs compared to uniform WSNs of the same size.

The problem of discretization (primarily the candidate sensor locations) is a limitation that may affect accuracy in real-world scenarios when exploring high-sensor density configurations. Additionally, the triggering mechanism could be refined by using calibrated detection thresholds that incorporate sensor descriptors accounting for weather and topography, as local conditions influence detection performance and thus affect the simulated arrival times used as input data.

Future work aims to demonstrate further the potential of our optimization approach and study special applications, problem formulations, constraints, and the protection of larger territories. While our framework focuses on optimizing sensor placement and comparing it to typical non-optimized configurations, future ideal systems will integrate hybrid EWDS components, such as UAVs, or new generation geostationary satellites, in areas where static sensors are not suitable and vice versa. We highlight this as a promising direction for further development. Recent research highlights the potential of integrating the Internet of Things (IoT) and machine learning technologies for early wildfire detection and monitoring, which can be included in our optimization framework. Some examples are the LoRaWan networking protocols for cost-effective, energy-efficient real-time surveillance in remote areas (Freira and Coutinho, 2024) and detection algorithms such as YOLOv8 to improve detection accuracy (Masram et al., 2024; Talaat and ZainEldin, 2023; Zhang, 2024).

More realistic triggering events could be based on atmospheric dispersion data of smoke particles, combustion chemicals, or other transportable wildfire observables that would allow earlier detection. Incorporating these transportable observables—individually or in combination—during optimization would reduce the attainable detection times and result in sensor arrangements better adjusted to real-world monitoring practices. These, however, are beyond the purpose of the current proof of concept demonstration.

It is also worth noting the opportunity to enhance post-detection suppression by integrating sequential sensor activations and other dynamic simulation data — e.g., to inform likely fire spread paths or constrain fire arrival at vulnerable locations following detection.

## CRediT authorship contribution statement

**Juan Luis Gómez-González:** Writing – original draft, Software, Methodology, Data curation, Conceptualization. **Effie Marcoulaki:** Writing – review & editing, Methodology, Conceptualization. **Alexis Cantizano:** Writing – review & editing, Methodology, Conceptualization. **Myrto Konstantinidou:** Writing – review & editing, Methodology, Conceptualization. **Raquel Caro:** Writing – review & editing, Methodology, Conceptualization. **Mario Castro:** Writing – review & editing, Methodology, Conceptualization.

## Software and data availability

The code developed for generating the results is open-sourced on the project's GitHubrepository. The project contains a Python script that prepares the different scenarios (with and without constraints) and instantiates the optimization problem (represented in a Pymoo problem class). To run the optimization experiment, we include the processed tabulated simulation data (ATs and BAs) as described in Section 2.3. The wildfire simulations used in this study are presented as well. The conda environment in which this project was developed is specified in the environment.yml file. This repository was created by Juan Luis Gómez-González (E-mail: juanlufisic@gmail.com) in 2024 and has program cords (64 KB) and sample data (107 MB). The experimental environment to conduct the optimization was as follows,

- OS: Microsoft Windows 11 Enterprise (Version 10.0.22631 Build 22631)
- CPU: 11th Gen Intel® Core™ i7-1185G7 @3.00 GHz
- RAM: 16.00 GB

## Declaration of competing interest

The authors declare that they have no known competing financial interests or personal relationships that could have appeared to influence the work reported in this paper.

## Acknowledgments

This work has been partially supported by Grant PID2022-140217NB-I00 funded by MCIN/AEI/10.13039/501100011033, and by "ERDF A way of making Europe".

## Appendix A. Supplementary data

Supplementary material related to this article can be found online at https://doi.org/10.1016/j.ecolind.2025.113509.

## References

Anderson, H.E., 1982. Aids to determining fuel models for estimating fire behavior. http://dx.doi.org/10.2737/INT-GTR-122, URL: https://www.fs.usda.gov/treesearch/pubs/6447.

Arca, B., Ghisu, T., Trunfio, G.A., 2015. GPU-accelerated multi-objective optimization of fuel treatments for mitigating wildfire hazard. J. Comput. Sci. 11, 258–268. http://dx.doi.org/10.1016/j.jocs.2015.08.009, URL: https://linkinghub.elsevier.com/retrieve/pii/S1877750315300120.

Argañaraz, J., Radeloff, V., Bar-Massada, A., Gavier-Pizarro, G., Scavuzzo, C., Bellis, L., 2017. Assessing wildfire exposure in the wildland-urban interface area of the mountains of central Argentina. J. Environ. Manag. 196, 499–510. http://dx.doi.org/10.1016/j.jenvman.2017.03.058, URL: https://linkinghub.elsevier.com/retrieve/pii/S0301479717302736.

Aslan, Y.E., Korpeoglu, I., Ulusoy, Ö., 2012. A framework for use of wireless sensor networks in forest fire detection and monitoring. Comput. Environ. Urban Syst. 36 (6), 614–625. http://dx.doi.org/10.1016/j.compenvurbsys.2012.03.002, URL: https://linkinghub.elsevier.com/retrieve/pii/S0198971512000300.

Azevedo, B.F., Brito, T., Lima, J., Pereira, A.I., 2021. Optimum sensors allocation for a forest fires monitoring system. Forests 12 (4), http://dx.doi.org/10.3390/f12040453, URL: https://www.mdpi.com/1999-4907/12/4/453.

Bayham, J., Yoder, J.K., Champ, P.A., Calkin, D.E., 2022. The economics of wildfire in the United States. Annu. Rev. Resour. Econ. 14 (1), 379–401. http://dx.doi.org/10.1146/annurev-resource-111920-014804, URL: https://www.annualreviews.org/doi/10.1146/annurev-resource-111920-014804.

Blank, J., Deb, K., 2020. Pymoo: Multi-objective optimization in Python. IEEE Access 8, 89497–89509. http://dx.doi.org/10.1109/ACCESS.2020.2990567, URL: https://ieeexplore.ieee.org/document/9078759/.

Bode, F., Reed, P., Reuschen, S., Nowak, W., 2019. Search space representation and reduction methods to enhance multiobjective water supply monitoring design. Water Resour. Res. 55 (3), 2257–2278. http://dx.doi.org/10.1029/2018WR023133, URL: https://agupubs.onlinelibrary.wiley.com/doi/10.1029/2018WR023133.

Calkin, D.E., Gebert, K.M., Jones, J.G., Neilson, R.P., 2005. Forest service large fire area burned and suppression expenditure trends, 1970–2002. J. For. 103 (4), 179–183. http://dx.doi.org/10.1093/jof/103.4.179, URL: https://academic.oup.com/jof/article/103/4/179/4598620.

Carrasco, J., Mahaluf, R., Lisón, F., Pais, C., Miranda, A., De La Barra, F., Palacios, D., Weintraub, A., 2023. A firebreak placement model for optimizing biodiversity protection at landscape scale. J. Environ. Manag. 342, 118087. http://dx.doi.org/10.1016/j.jenvman.2023.118087, URL: https://linkinghub.elsevier.com/retrieve/pii/S0301479723008757.

Carta, F., Zidda, C., Putzu, M., Loru, D., Anedda, M., Giusto, D., 2023. Advancements in forest fire prevention: A comprehensive survey. Sensors 23 (14), 6635. http://dx.doi.org/10.3390/s23146635, URL: https://www.mdpi.com/1424-8220/23/14/6635.

Castro, I., Salas-González, R., Fidalgo, B., Farinha, J.T., Mendes, M., 2024. Optimising forest management using multi-objective genetic algorithms. Sustain. 16 (23), http://dx.doi.org/10.3390/su162310655, URL: https://www.mdpi.com/2071-1050/16/23/10655.

Chan, C.C., Alvi, S.A., Zhou, X., Durrani, S., Wilson, N., Yebra, M., 2023. IoT ground sensing systems for early wildfire detection: Technologies, challenges and opportunities. ArXiv Preprint arXiv:2312.10919. URL: https://arxiv.org/abs/2312.10919.

Chen, W., Sivaramakrishnan, E.P., Dilkina, B., 2022. Landscape optimization for prescribed burns in wildfire mitigation planning. In: Proceedings of the 5th ACM SIGCAS/SIGCHI Conference on Computing and Sustainable Societies. COMPASS '22, Association for Computing Machinery, New York, NY, USA, pp. 429–438. http://dx.doi.org/10.1145/3530190.3534816.

Coen, J.L., Cameron, M., Michalakes, J., Patton, E.G., Riggan, P.J., Yedinak, K.M., 2013. WRF-fire: Coupled weather–wildland fire modeling with the weather research and forecasting model. J. Appl. Meteorol. Clim. 52 (1), 16–38. http://dx.doi.org/10.1175/JAMC-D-12-023.1, URL: https://journals.ametsoc.org/view/journals/apme/52/1/jamc-d-12-023.1.xml.

Copernicus Climate Change Service (C3S), 2018. ERA5 hourly data on single levels from 1940 to present. http://dx.doi.org/10.24381/CDS.ADBB2D47, URL: https://cds.climate.copernicus.eu/doi/10.24381/cds.adbb2d47.

Copernicus Emergency Management Service (CEMS), 2019. Fire danger indices historical data from the Copernicus emergency management service. http://dx.doi.org/10.24381/cds.0e89c522, URL: https://ewds.climate.copernicus.eu/datasets/cems-fire-historical-v1?tab=overview.

Dampage, U., Bandaranayake, L., Wanasinghe, R., Kottahachchi, K., Jayasanka, B., 2022. Forest fire detection system using wireless sensor networks and machine learning. Sci. Rep. 12 (1), 46. http://dx.doi.org/10.1038/s41598-021-03882-9, URL: https://www.nature.com/articles/s41598-021-03882-9.

Dang, H., Lü, Y., Guo, J., Wu, X., 2024. Multi-scenario simulation can contribute to identify priorities for regional ecological corridors conservation. Ecol. Indic. 165, 112166. http://dx.doi.org/10.1016/j.ecolind.2024.112166, URL: https://www.sciencedirect.com/science/article/pii/S1470160X2400623X.

De Diego, J., Fernández, M., Rúa, A., Kline, J.D., 2023. Examining socioeconomic factors associated with wildfire occurrence and burned area in Galicia (Spain) using spatial and temporal data. Fire Ecol. 19 (1), 18. http://dx.doi.org/10.1186/s42408-023-00173-8, URL: https://fireecology.springeropen.com/articles/10.1186/s42408-023-00173-8.

De Oliveira, G., Mataveli, G., Stark, S.C., Jones, M.W., Carmenta, R., Brunsell, N.A., Santos, C.A.G., Da Silva Junior, C.A., Cunha, H.F.A., Da Cunha, A.C., Dos Santos, C.A.C., Stewart, H., Boanada Fuchs, V., Hellenkamp, S., Artaxo, P., Alencar, A.A.C., Moutinho, P., Shimabukuro, Y.E., 2023. Increasing wildfires threaten progress on halting deforestation in Brazilian Amazonia. Nat. Ecol. Evol. http://dx.doi.org/10.1038/s41559-023-02233-3, URL: https://www.nature.com/articles/s41559-023-02233-3.

Deb, K., Pratap, A., Agarwal, S., Meyarivan, T., 2002. A fast and elitist multiobjective genetic algorithm: NSGA-II. IEEE Trans. Evol. Comput. 6 (2), 182–197. http://dx.doi.org/10.1109/4235.996017, URL: http://ieeexplore.ieee.org/document/996017/.

Dryad Networks, 2025. Silvanet - AI wildfire detection in minutes. https://www.dryad.net/silvanet. (Accessed 21 March 2025).

Dupuy, J.-l., Fargeon, H., Martin-StPaul, N., Pimont, F., Ruffault, J., Guijarro, M., Hernando, C., Madrigal, J., Fernandes, P., 2020. Climate change impact on future wildfire danger and activity in southern europe: a review. Ann. For. Sci. 77 (2), 35. http://dx.doi.org/10.1007/s13595-020-00933-5, URL: https://annforsci.biomedcentral.com/articles/10.1007/s13595-020-00933-5.

Encyclopaedia Britannica, 2024. Beaufort scale. Encycl. Br. URL: https://www.britannica.com/science/Beaufort-scale. (Accessed 14 February 2025).

European Forest Fire Information System (EFFIS), 2007. Fire danger forecast. URL: https://forest-fire.emergency.copernicus.eu/about-effis/technical-background/fire-danger-forecast. (Accessed 14 February 2025).

Finney, M.A., 1998. FARSITE: Fire area simulator-model development and evaluation. In: Res. Pap. RMRS-RP-4, Revised 2004. Vol. 47, U.S. Department of Agriculture, Forest Service, Rocky Mountain Research Station, Ogden, UT, p. 4. http://dx.doi.org/10.2737/RMRS-RP-4, URL: http://www.fs.usda.gov/treesearch/pubs/4617.

Freira, D., Coutinho, C., 2024. Wildfire detection based on IoT technology. In: 2024 8th International Symposium on Multidisciplinary Studies and Innovative Technologies. ISMSIT, IEEE, Ankara, Turkiye, pp. 1–6. http://dx.doi.org/10.1109/ISMSIT63511.2024.10757256.

Gebert, K.M., Calkin, D.E., Yoder, J., 2007. Estimating suppression expenditures for individual large wildland fires. West. J. Appl. For. 22 (3), 188–196. http://dx.doi.org/10.1093/wjaf/22.3.188, URL: https://academic.oup.com/wjaf/article/22/3/188/4717756.

Generalitat Conselleria de Medio Ambiente, Infraestructuras y Territorio, 2015. Sistema integrado de gestión de incendios forestales (SIGIF), informes post incendio compendio anual 2012 - 2013 [Integrated forest fire management system (SIGIF), post-fire reports annual compendium 2012 – 2013]. URL: https://prevencionincendiosgva.es/Inicio. (Accessed 14 February 2025).

Gobierno de Castilla y León, 1999. Plan especial de emergencias por incendios forestales de Castilla y León (INFOCAL) [Special emergency plan for forest fire in Castilla y León]. URL: https://medioambiente.jcyl.es/web/es/medio-natural/infocal.html. (Accessed 14 February 2025).

Gómez-González, J.L., Cantizano, A., Caro-Carretero, R., Castro, M., 2024. Leveraging national forestry data repositories to advocate wildfire modeling towards simulation-driven risk assessment. Ecol. Indic. 158, 111306. http://dx.doi.org/10.1016/j.ecolind.2023.111306, URL: https://linkinghub.elsevier.com/retrieve/pii/S1470160X23014486.

Granda, B., Vitoriano, B., 2024. The team orienteering problem with variable time windows. Int. Trans. Oper. Res. itor.13570. http://dx.doi.org/10.1111/itor.13570, URL: https://onlinelibrary.wiley.com/doi/10.1111/itor.13570.

Hantson, S., Andela, N., Goulden, M.L., Randerson, J.T., 2022. Human-ignited fires result in more extreme fire behavior and ecosystem impacts. Nat. Commun. 13 (1), 2717. http://dx.doi.org/10.1038/s41467-022-30030-2, URL: https://www.nature.com/articles/s41467-022-30030-2.

Heyns, A., Du Plessis, W., Kosch, M., Hough, G., 2019. Optimisation of tower site locations for camera-based wildfire detection systems. Int. J. Wildland Fire 28 (9), 651. http://dx.doi.org/10.1071/WF18196, URL: http://www.publish.csiro.au/?paper=WF18196.

Hoffman, K.M., Davis, E.L., Wickham, S.B., Schang, K., Johnson, A., Larking, T., Lauriault, P.N., Quynh Le, N., Swerdfager, E., Trant, A.J., 2021. Conservation of earth's biodiversity is embedded in indigenous fire stewardship. Proc. Natl. Acad. Sci. 118 (32), e2105073118. http://dx.doi.org/10.1073/pnas.2105073118, URL: https://pnas.org/doi/full/10.1073/pnas.2105073118.

Jaszkiewicz, A., 2004. On the computational efficiency of multiple objective metaheuristics. the knapsack problem case study. European J. Oper. Res. 158 (2), 418–433. http://dx.doi.org/10.1016/j.ejor.2003.06.015, URL: https://linkinghub.elsevier.com/retrieve/pii/S0377221703004946.

Karimi, N., Mahler, P., Beverly, J.L., 2024. Optimizing fuel treatments for community wildfire mitigation planning. J. Environ. Manag. 370, 122325. http://dx.doi.org/10.1016/j.jenvman.2024.122325, URL: https://linkinghub.elsevier.com/retrieve/pii/S0301479724023119.

Kaur, P., Kaur, K., Singh, K., Kim, S., 2023. Early forest fire detection using a protocol for energy-efficient clustering with weighted-based optimization in wireless sensor networks. Appl. Sci. 13 (5), 3048. http://dx.doi.org/10.3390/app13053048, URL: https://www.mdpi.com/2076-3417/13/5/3048.

Kizilkaya, B., Ever, E., Yatbaz, H.Y., Yazici, A., 2022. An effective forest fire detection framework using heterogeneous wireless multimedia sensor networks. ACM Trans. Multimed. Comput. Commun. Appl. 18 (2), 1–21. http://dx.doi.org/10.1145/3473037, URL: https://dl.acm.org/doi/10.1145/3473037.

Liang, J., Calkin, D.E., Gebert, K.M., Venn, T.J., Silverstein, R.P., 2008. Factors influencing large wildland fire suppression expenditures. Int. J. Wildland Fire 17 (5), 650. http://dx.doi.org/10.1071/WF07010, URL: http://www.publish.csiro.au/?paper=WF07010.

Linn, R., Reisner, J., Colman, J.J., Winterkamp, J., 2002. Studying wildfire behavior using FIRETEC. Int. J. Wildland Fire 11 (4), 233. http://dx.doi.org/10.1071/WF02007, URL: http://www.publish.csiro.au/?paper=WF02007.

Lloret, J., Garcia, M., Bri, D., Sendra, S., 2009. A wireless sensor network deployment for rural and forest fire detection and verification. Sensors 9 (11), 8722–8747. http://dx.doi.org/10.3390/s91108722, URL: http://www.mdpi.com/1424-8220/9/11/8722.

Machado-Silva, F., Libonati, R., Melo de Lima, T.F., Bittencourt Peixoto, R., de Almeida França, J.R., de Avelar Figueiredo Mafra Magalhães, M., Lemos Maia Santos, F., Abrantes Rodrigues, J., DaCamara, C.C., 2020. Drought and fires influence the respiratory diseases hospitalizations in the Amazon. Ecol. Indic. 109, 105817. http://dx.doi.org/10.1016/j.ecolind.2019.105817, URL: https://www.sciencedirect.com/science/article/pii/S1470160X19308118.

Mack, M.C., Walker, X.J., Johnstone, J.F., Alexander, H.D., Melvin, A.M., Jean, M., Miller, S.N., 2021. Carbon loss from boreal forest wildfires offset by increased dominance of deciduous trees. Sci. 372 (6539), 280–283. http://dx.doi.org/10.1126/science.abf3903, URL: https://www.science.org/doi/10.1126/science.abf3903.

Marshall, E., Elliot-Kerr, S., McColl-Gausden, S.C., Penman, T.D., 2023. Costs of preventing and supressing wildfires in Victoria, Australia. J. Environ. Manag. 344, 118606. http://dx.doi.org/10.1016/j.jenvman.2023.118606, URL: https://linkinghub.elsevier.com/retrieve/pii/S0301479723013944.

Masram, B.Y., Kangale, Y., Mendhe, A., Mishra, A., Shindekar, N., Pathade, A.G., 2024. A smart forest fire detection and notification system using IoT and machine learning. In: 2024 International Conference on Electrical Electronics and Computing Technologies. ICEECT, IEEE, Greater Noida, India, pp. 1–6. http://dx.doi.org/10.1109/ICEECT61758.2024.10739106.

Meier, S., Elliott, R.J., Strobl, E., 2023. The regional economic impact of wildfires: Evidence from Southern Europe. J. Environ. Econ. Manag. 118, 102787. http://dx.doi.org/10.1016/j.jeem.2023.102787, URL: https://linkinghub.elsevier.com/retrieve/pii/S0095069623000050.

Ministerio del Interior, Secretaría General Técnica, Dirección General de Protección Civil y Emergencias, 2014. Plan Estatal de protección civil para emergencias por incendios forestales [State Civil Protection Plan for Forest Fire Emergencies]. URL: http://publicacionesoficiales.boe.es. (Accessed 14 February 2025).

Ministerio para la Transición Ecológica y el Reto Demográfico (MITECO), 2019. Estadísticas generales de incendios forestales (EGIF) [General Statistics on Forest Fires]. URL: https://www.miteco.gob.es/es/biodiversidad/temas/incendios-forestales/estadisticas-datos.aspx. (Accessed 14 February 2025).

Mohapatra, A., Trinh, T., 2022. Early wildfire detection technologies in practice—A review. Sustain. 14 (19), 12270. http://dx.doi.org/10.3390/su141912270, URL: https://www.mdpi.com/2071-1050/14/19/12270.

Molina-Terrén, D.M., Xanthopoulos, G., Diakakis, M., Ribeiro, L., Caballero, D., Delogu, G.M., Viegas, D.X., Silva, C.A., Cardil, A., 2019. Analysis of forest fire fatalities in Southern Europe: Spain, Portugal, Greece and Sardinia (Italy). Int. J. Wildland Fire 28 (2), 85. http://dx.doi.org/10.1071/WF18004, URL: http://www.publish.csiro.au/?paper=WF18004.

Ottmar, R.D., 2014. Wildland fire emissions, carbon, and climate: Modeling fuel consumption. Forest Ecol. Manag. 317, 41–50. http://dx.doi.org/10.1016/j.foreco.2013.06.010, URL: https://linkinghub.elsevier.com/retrieve/pii/S0378112713003782.

Pan, S., Gan, L., Jung, J., Yu, W., Roy, A., Diao, L., Jeon, W., Souri, A.H., Gao, H.O., Choi, Y., 2023. Quantifying the premature mortality and economic loss from wildfire-induced PM2.5 in the contiguous U.S.. Sci. Total Environ. 875, 162614. http://dx.doi.org/10.1016/j.scitotenv.2023.162614, URL: https://linkinghub.elsevier.com/retrieve/pii/S0048969723012305.

Plucinski, M.P., 2019. Fighting flames and forging firelines: Wildfire suppression effectiveness at the fire edge. Curr. For. Rep. 5 (1), 1–19. http://dx.doi.org/10.1007/s40725-019-00084-5, URL: http://link.springer.com/10.1007/s40725-019-00084-5.

Prichard, S.J., Karau, E.C., Ottmar, R.D., Kennedy, M.C., Cronan, J.B., Wright, C.S., Keane, R.E., 2014. Evaluation of the CONSUME and FOFEM fuel consumption models in pine and mixed hardwood forests of the eastern United States. Can. J. Forest Res. 44 (7), 784–795. http://dx.doi.org/10.1139/cjfr-2013-0499, URL: http://www.nrcresearchpress.com/doi/10.1139/cjfr-2013-0499.

Prieto Herráez, D., Asensio Sevilla, M.I., Ferragut Canals, L., Cascón Barbero, J.M., Morillo Rodríguez, A., 2017. A GIS-based fire spread simulator integrating a simplified physical wildland fire model and a wind field model. Int. J. Geogr. Inf. Sci. 31 (11), 2142–2163. http://dx.doi.org/10.1080/13658816.2017.1334889, URL: https://www.tandfonline.com/doi/full/10.1080/13658816.2017.1334889.

Pyri, 2025. Pyri - wildfire intelligence platform. https://www.pyri.io/. (Accessed 10 March 2025).

Rodrigues, M., Alcasena, F., Vega-García, C., 2019. Modeling initial attack success of wildfire suppression in Catalonia, Spain. Sci. Total Environ. 666, 915–927. http://dx.doi.org/10.1016/j.scitotenv.2019.02.323, URL: https://linkinghub.elsevier.com/retrieve/pii/S0048969719308319.

Sairi, A., Labed, S., Miles, B., Kout, A., 2023. A review on early forest fire detection using IoT-enabled WSN. In: 2023 International Conference on Advances in Electronics, Control and Communication Systems (ICAECCS). IEEE, BLIDA, Algeria, pp. 1–6. http://dx.doi.org/10.1109/ICAECCS56710.2023.10104887, URL: https://ieeexplore.ieee.org/document/10104887/.

Skretas, A., Gyftakis, S., Marcoulaki, E., 2022. A demonstration of sustainable pipeline routing optimization using detailed financial and environmental assessment. J. Clean. Prod. 362, 132305. http://dx.doi.org/10.1016/j.jclepro.2022.132305, URL: https://linkinghub.elsevier.com/retrieve/pii/S0959652622019096.

Sullivan, A.L., 2009. Wildland surface fire spread modelling, 1990 - 2007. 2: Empirical and quasi-empirical models. Int. J. Wildland Fire 18 (4), 369. http://dx.doi.org/10.1071/WF06142, URL: http://www.publish.csiro.au/?paper=WF06142.

Talaat, F.M., ZainEldin, H., 2023. An improved fire detection approach based on YOLOv8 for smart cities. Neural Comput. Appl. 35 (14), 20939–20954. http://dx.doi.org/10.1007/s00521-023-08809-1.

Tymstra, C., Bryce, R., Wotton, B., Taylor, S., Armitage, O., et al., 2010. Development and Structure of Prometheus: the Canadian Wildland Fire Growth Simulation Model. Information Report NOR-X-417, Natural Resources Canada, Canadian Forest Service, Northern Forestry Centre, Edmonton, AB, URL: https://publications.gc.ca/site/eng/380448/publication.html.

Van Der Werf, G.R., Randerson, J.T., Giglio, L., Van Leeuwen, T.T., Chen, Y., Rogers, B.M., Mu, M., Van Marle, M.J.E., Morton, D.C., Collatz, G.J., Yokelson, R.J., Kasibhatla, P.S., 2017. Global fire emissions estimates during 1997–2016. Earth Syst. Sci. Data 9 (2), 697–720. http://dx.doi.org/10.5194/essd-9-697-2017, URL: https://essd.copernicus.org/articles/9/697/2017/.

Verma, S., Kaur, S., Rawat, D.B., Xi, C., Alex, L.T., Zaman Jhanjhi, N., 2021. Intelligent framework using IoT-based WSNs for wildfire detection. IEEE Access 9, 48185–48196. http://dx.doi.org/10.1109/ACCESS.2021.3060549, URL: https://ieeexplore.ieee.org/document/9358205/.

Wagenbrenner, N.S., Forthofer, J.M., Lamb, B.K., Shannon, K.S., Butler, B.W., 2016. Downscaling surface wind predictions from numerical weather prediction models in complex terrain with WindNinja. Atmospheric Chem. Phys. 16 (8), 5229–5241. http://dx.doi.org/10.5194/acp-16-5229-2016, URL: https://acp.copernicus.org/articles/16/5229/2016/.

Yick, J., Mukherjee, B., Ghosal, D., 2008. Wireless sensor network survey. Comput. Netw. 52 (12), 2292–2330. http://dx.doi.org/10.1016/j.comnet.2008.04.002, URL: https://linkinghub.elsevier.com/retrieve/pii/S1389128608001254.

Zhang, M., 2024. An improved fire detection algorithm based on YOLOv8 integrated with DGIConv, FourBranchAttention and GSIoU. HighTech Innov. J. 5 (3), 677–689. http://dx.doi.org/10.28991/HIJ-2024-05-03-09, URL: https://doi.org/10.28991/HIJ-2024-05-03-09.